DATA DOCUMENTATION FOR THE BARE SOIL EXPERIMENT AT THE UNIVERSITY OF ARKANSAS JUNE - AUGUST 1980

by

Ali M. Sadeghi

W. P. Waite, Principal Investigator

NASA Grant No. NAG 5-20

Goddard Space Flight Center

Department of Electrical Engineering
University of Arkansas
Fayetteville, Arkansas 72701

March 1984

TABLE OF CONTENTS

LIST OF TABLES

LIST OF FIGURES

LIST OF FIGURES

LIST OF FIGURES

INTRODUCTION

Water contained in the soil surface plays an important role in infiltration, runoff, heat transfer, evapotranspiration, seed germination, and many other aspects of Agriculture and hydrologic systems. Due to the direct contact to the atmosphere, the status of this moisture is highly dynamic. The variation is mainly related to the soil type and the microclimalological parameters adjacent to the soil surface.

Knowledge of the quantity of the moisture stored at this region of the soil can be very useful in predicting crop yield, and will increase the efficiency of water use management. Several methods have been followed to estimate the amount of this moisture. With the continuous increase in interest to manage this resource properly, remote sensing offers a potentially accurate technique to evaluate the moisture stored at this region of the soil (4).

Three spectral regions are used in remote sensing, visible and near-infrared, thermal infrared, and microwave. The microwave region has been used to study the moisture content status near the soil surface (5).

The dependence of microwave emissivity of the soil on the soil moisture content has been studied at the Institude of Rural Engineering in 1977 and 1978 (5).

Peake (1959), Lundien (1966) have stated that the microwave emission of the soil is highly affected by the moisture content of the soil. The influence of the soil moisture on the microwave reflectivity at the soil surface is mostly through the magnitude of the complex dielectric constant of soil (2 to 5 for dry soil and near 80 for pure water) (5).

Since 1971, many measurements have been conducted on the complex dielectric constant of soils as a function of soil moisture content. Amoung these measurements, some have shown the existence of a strong dependence for the functional relationships between soil moisture content and the magnitude of the dielectric constant, on the soil type (7).

The primary objective of this study is to evaluate the relationships between soil moisture and reflectivity of a bare soil, using microwave techniques. A drainage experiment was conducted on a Captina silt loam in cooperation with personal in the Electrical Engineering Department. Measurements included, soil moisture pressures at various depths, neutron probe measurements, gravimetric moisture samples, and reflectivity of the soil surface at selected frequencies including 1.5 and 6.0 GH_z and at the incident angle of 45°. All measurements were made in conjuction with that of reflectivity data.

METHODS AND MATERIALS

Plot Preparation

The experimental site was located on the west side of the main Experiment Station, at Fayetteville in an area mapped as Captina silt loam. The morphological description of the Captina soil at the site is given in Appendix A, Table 1.

A plot with dimensions of 3.66 x 3.05m^2 was constructed by removing the grass vegetation and confining the area with a wooden frame. The boards of the frame were placed into the soil to a depth of approximately 20cm, leaving 10cm above the soil surface, this was designed to confine the soil moisture redistribution within the plot area. A drainage ditch also was added around the plot to detect lateral movement of water caused by rainfall into the plot area. A wooden frame roof consisting of three pieces of corrugated fiberglass was constructed in order to keep out precipitation after the saturation of the plot and during the drying cycle. The roof was made of three sections so that it could be easily removed to allow access to the instruments used to monitor soil water movements. The roof was slopped at 10% to prevent leakage caused by the accumulation of water from the rainfall.

Experimental Instrumentation

After the initial preparation, the plot was instrumented with a bistatic reflectometer for soil reflectivity measurements. Three banks of tensiometers (macro, and microtensiometers) with mercury manometers were positioned at 1, 3, 5, 10cm depths for microtensiometers, and 15cm increments ranging from soil depth of 15cm to 137cm for macrotensiometers. Each bank contained one neutron probe access tube in order to complement

the tensiometers (Figure 1, Appendix B).

The reflectivity data were obtained by installation of the transmitter and receiver antennas at the north and south sides of the plot. The height of the antennas from the ground surface was approximately 3m, and was adjusted to an angle of 45° through the soil target (Fig. 2). The band widths of the two antennas ranged from the frequency of 1 to 2 GH_z and from 4 to 8 GH_z. The receivers were furnished with a network analyzer as a ratiometer and an X-Y plotter to give a continuous recording system. The reflectometer system was calibrated with a thin sheet of aluminum. This aluminum sheet was placed over the soil surface and was removed after the reflectivities were taken. The ratio of the relectivity from the aluminum sheet and the reflectivity from the bare soil elminates system parameters.

Tensiometer data along with the access tubes measurements were used to determine the soil moisture potentials and corresponding moisture contents at various depths for each bank. Three banks of tensiometers and access tubs were placed in the plot as shown in Figure 1. In order to minimize the effect of the plot boundary on the tensiometers, attempts were made to keep the distance between tensiometers and plot boundary more than 15cm, the same distance also was used to locate the access tubes and the tensiometers. This was done to detect the effects of the water in the tensiometers on the neutron probe readings. Figure 3 App. B shows the cross-sectional area of each bank and indicates the location of the two types of tensiometers which were used in this study. Due to the importance of the soil moisture status at the surface, micro-tensiometers were placed with small increments at 1, 3, 5, 10cm soil depths.

Final Plot Preparation

After the plot was instrumented the soil surface was tilled lightly and leveled. This was done to have a relatively smooth surface. Water then was applied to the plot through a perforated plastic garden hose. In order to keep water from ponding, a steady state was established between the application rate and infiltration rate of water in the plot. The application rate was found to be approximately 1.4 centimeters of water in an hour. The wetting process at this rate was continued until the plot appeared saturated.

Soil Samples

Five soil cores with the dimensions 6cm x 5cm and five slurry soil samples were taken from the depths corresponding to the tensiometer positions. Soil core samples were used to determine saturated, hydraulic conductivity, moisture retention characteristics for pressures less than one bar, and bulk density. Soil slurry samples were used to determine particle density, particle size distribution, and moisture retention characteristics for pressures from one to fifteen bars.

Characterization of Soil Physical Properties

Immediately after the plot was considered to be saturated, time zero, the time when all surface water infiltrated the soil was assumed to be the start of the drying cycle. The plot then was allowed to dry.

Measurements taken included reflectivity at frequencies, 1.5, and 0.0 GH_z, tensiometer readings, neutron probe measurements, and soil gravimetric samples. At the initiation of the drying cycle, the soil was nearly saturated and the rate of water movement decreased sharply with time. Therefore, measurements of the water status were taken every

two hours for approximately three days. As the soil dried by evaporation and drainage, the frequency of the measurements were reduced to three times a day, morning, solar noon, and late afternoon. Later the number of measurements was reduced to two times a day, and finally to one daily measurement in the afternoon. There were three drying cycles, the first drying cycle was stopped in the fourth day due to a heavy rain, which caused flooding in the plot. The second and third drying cycles were complete cycles. The data obtained from each cycle included soil samples, tensiometer readings, and soil surface reflectivities. Soil Core Samples were used to determine saturated hydraulic conductivity by the constant head method using Darcy's Law as follow.

$$K = QL/At\Delta H \qquad [1]$$

Soil moisture retention characteristics at pressures ranging from 0-1 bar, using the pressure plate method. In order to show the unformity of the Captina soil, soil water contents were plotted against the natural logarithm of matric potentials. The regression line is defined by the following equation.

$$_{m} = A \exp[\ \theta_{v}] \qquad [2]$$

Bulk density was determined by dividing the weight of dry soil in each core by its volume. The slurry soil samples were used to determine particle density using the pycnometer method, particle size distribution by mechanical analysis, and to determine soil moisture characteristics for pressure more than one bar.

Unsaturated hydraulic conductivity was determined from the hydraulic gradient and soil water flux. Hydraulic gradients were obtained from tensiometer measurements at various soil depths. The flux of water was calculated by determining the position of the "zero flux plane". In a soil profile which is subjected to both evaporation and drainage the zero flux plane will separate the portion of soil water which moves upward in response to evaporation from that which moves downward in response to drainage. There is no water movement across this plane. The flux of water at any depth, is obtained by integrating the rate of change in moisture content with time for a distance from the zero flux plane to the depth in question. The position of the plane of zero flux moves downward as the soil profile dries. The hydraulic conductivity can be determined by dividing the soil water flux by the potential gradient as follows;

$$K(\theta)_a = [\int_{z_o}^{z_a} (\partial\theta/\partial t)dz] \div (\partial\Psi/\partial z)_{z_a} \qquad [3]$$

$$K(\theta)_b = [\int_{z_o}^{z_b} (\partial\theta/\partial t)dz] \div (\partial\Psi/\partial z) \qquad [4]$$

where a and b are the depths in soil profile above and below the depth of zero flux plane, z_o and $K(\theta)_a$, $K(\theta)_b$ are the hydraulic conductivities corresponding to the water contents at specified depths a and b (1).

Functional relationships were developed between hydraulic conductivity data and both volumetric water content, θ_v and the deficit volumetric water content from the saturation, $(\theta_s - \theta_v)$. The equations are described as follows.

$$K = K_o \exp[\beta\theta_v] \quad [5]$$

$$K = K_o \exp[\beta(\theta_s - \theta_v)] \quad [6]$$

Daily flux of water across the soil surface or evaporation after each day was calculated, using Eq. [3]. The evaporation rates were then plotted as a function of time in day to indicate the separation of the theoretical two stages of evaporation.

Soil Water Diffusivity

The soil water diffusivity, D, for Captina silt loam was calculated depending upon the water content in two ways, for the water contents during the first stage of evaporation, D was determined from the K at that water content and the slope of the water retention curve (specific water capacity). The relation between D, K, and specific water capacity is described as follows.

$$D = -K(\theta_v)(\partial\Psi_m/\partial\theta) \quad [7]$$

For the water content at the beginning of the second stage of evaporation or less, D was determined from the solution of unsaturated flow equation described by Fick's first law.

$$F = -D\, \partial\theta/\partial x \qquad [8]$$

where, F is the flux of water (cm^3/cm^2 sec.).

Combining Eq. [8] with the law of conservation of mass gives the equation which has become known as Fick's second law.

$$\partial\theta/\partial t = \partial/\partial x[D(\theta)\, \partial\theta/\partial x] \qquad [9]$$

According to Crank, (3) Eq. [9] can be solved analytically for a semi-infinite slab with constant diffusivity, D, to calculate flux at the boundary, the solution is as follows,

$$F = (\theta_i - \theta_o)\, D/\pi t)^{\frac{1}{2}} \qquad [10]$$

where: θ_i = the initial water content, water content at the beginning of the stage II.

θ_o = the water content at the soil surface, assumed to be zero.

Cumulative evaporation, E, will be obtained by integrating the Eq. [10] with respect to time.

$$E = (\theta_i - \theta_o)(D\, t/\pi)^{\frac{1}{2}} \qquad [11]$$

For further simplification we assume a coefficient, A to be,

$$A = 2(\theta_i - \theta_o)(D/\pi)^{\frac{1}{2}} \qquad [12]$$

$$A = 2(\theta_i - \theta_o)(D/\pi)^{\frac{1}{2}} \quad [12]$$

Then

$$E = At^{-\frac{1}{2}} \quad [13]$$

In order to calculate the diffusivity for the period of stage II, the cumulative evaporations were plotted against the square root of time in days, coefficient A is the slope of the regression line. Knowing this coefficient, and the values of θ_i, θ_o, the soil water diffusivity was calculated using Eq. [8].

Soil Reflectivity

Reflectivity of the soil during this experiment are presented in Appendix A, Table 9-11. The type of reflectometer frequency of the band width, and the incident angle were discussed in the Experimental Instrumentation. Data obtained at various frequencies were converted to reflectivi. It is to be noted that, reflection coefficient is a square root of the reflectivity value.

RESULTS AND DISCUSSION

Soil Profile Description

A soil profile description made at the study site is given in Table 1, Appendix A. The soil is in an area mapped as Captina silt loam. The Captina soil is described as a moderately well drained, slowly permeable, and dominated in the lower horizons by a firm, brittle, fragipan. It is classified as a Typic Fragiudalf with a predominate texture of silt loam.

The most distinguishing characteristic of the Captina soil at the study site is the presence of a fragipan located at depths ranging from 70 to 120cm. The boundary between fragipan and nonfragipan was found to be wavy (tong shapped), which will cause a large variabilities in the water transport data obtained within this region of the soil profile. The Ap horizon, the first 18cm of the top soil, has a fine granular structure, where as in Ap2 a massive structure was observed from 18 to 30cm. The B horizon starts at the 30cm depth, where a sudden change in color from brown to yellowish brown was observed. As the data in Table 2, Appendix A shows at the beginning of the B horizon contains a greater clay content; the maximum clay content was in the depth range from 88 to 93cm in the B23t horizon.

Bulk Density

The bulk density values range from 1.27 gm/cm^3, the lowest value in the Ap horizon, to a value of 1.41 gm/cm^3 in the same horizon. This increase in bulk density within the same horizon could be due to the presence of a plow pan. Bulk density remained essentially constant around 1.40 gm/cm^3 along the Ap2 horizon starting at 18cm to the end of

the B1 horizon at 45cm. From B21t at 45cm, the values of bulk densities increase to a maximum in the middle of the fragipan. The maximum bulk density was 1.64 gm/cm^3 which is considered to be a fairly high for silt loam soils. Finally the overall average bulk density of the soil profile was 1.47 gm/cm^3. This compare favorably with the average bulk density of 1.51 gm/cm^3 found in 1976 by Paetzold on the same soil but at a different location. The data in Fig. 4 shows the variation in bulk density.

Particle Density

The data in Fig. 5, Appendix B shows the variation of particle density as a function of soil depth. Generally the values of particle density are nearly constant in a soil profile which is morphologically uniform. As the data in Fig. 5 represents the minimum value for particle density in Captina soil was 2.49 gm/cm^3 at the soil surface. This value is generally considered to be low which is probably due to the presence of organic matter since the particle density of organic matter is low. The values of particle density increased to the 30cm depth and remained fairly constant in a range from 2.61 to 2.64 gm/cm^3.

Porosity

Porosity ranged from 0.49 cm^3/cm^3 in the Ap to 0.374 in B23t & BX1 norixon. Data in Table 2 in Appendix A indicates that if particle density is fairly constant, the variation of porosity in the soil profile is inversely related to the magnitude of the bulk density.

Particle Size Distribution

Particle size distribution was determined using mechanical analyses. The data in Fig. 6 Appendix B shows the accumulative distribution of particle size throughout the soil profile. The Captina soil is dominated

by a large quantity of silt. The second largest textural component was clay, the lowest amount of clay of 10% was found at the surface in Ap horizon, and the highest quantity of clay of 30% in the B23t horizon. The sand fraction was the lowest percentage size fraction in the profile and varied from 25% in Ap to 18% in BX2. The maximum of 40% of sand was found in the B24t, which is probably due to the fact that this soil is formed from the weathering of sandstone. The data in Tables 2 and 3 in Appendix A show selective physical properties and particle size distributions of the Captina soil.

Mositure Retention Characteristics

The data in Fig. 7 and 8 in Appendix B represent the functional relationships between moisture content and matric potentials less than one bar. The maximum moisture content of 0.432 cm^3/cm^3 was found at saturation in the Ap horizon, and the minimum value of 0.271 cm^3/cm^3 at 1 bar pressure in the B21t horizon. The BX2 horizon retained relatively lower amounts of moisture than the horizons above and below. This is possibly due to the presence of the fragipan in this horizon. In order to find out if the data fit the equation [2], the moisture retention data were transfered into semi log plots. The data in Fig. 9 and 10 describe this functional relation for Ap and B1 horizon. The correlation values range from 0.993 at the surface to 0.976 at B24t horizon. Higher values for slope of the regression lines were obtained in deeper horizons which is possibly due to the accumulation of the clay particles along the soil profile. The higher the slope of the regression line, the higher the dependence of water content on matric potential. The data in Table 4 in Appendix A represents the correlation coefficient values, intercepts, and slope of the regression lines along with the mathematical model for each soil horizon.

Soil Water Status

Evaluation of the soil water relations is the most important step in interpretation of the functional relationships between soil moisture and reflectivity of the soil, especially near the soil surface. The data in Appendix B, Fig. 11 through 13 represent the daily mean volumetric water contents, daily total hydraulic heads, and diurnal variation in matric potentials as a function of soil depth. A comparison between the broken line (Theoretical saturation line), and the solid line (line representing the variation in water content at the beginning of the drainage cycle) on Fig. 11 indicates that the plot was nearly saturated. The data in Fig. 12, illustrate the variation of daily total hydraulic head as a function of depth. A positive slope indicates water moving upward, while a negative slope indicates the downward movement of water. The dotted line in Fig. 12 represents the separation of upward movement of water from downward. Data in Fig. 13 demonstrate diurnal changes in soil matric potential at the selected depths, the maximum variation was observed in the first few days at the beginning of the drainage cycle, especially for 1, 3, and 5cm depths.

The data in Fig. 14 Appendix B demonstrate the rate of drainage in comparison with the rate of evaporation during the drainage cycle. The average drainage rate decreases from 2.56cm/day to 0.712cm/day within 24 hours, where as a slow change in drainage rate was observed after the first day of the drainage cycle. From the second day during the drying process, the rate of evaporation and the rate of drainage were decreasing uniformely. Data in Table 5 in Appendix A represent the evaporation rate across the 1cm depth and the drainage rate across 122cm

depth of the soil profile during the second drainage cycle (longest drainage cycle).

Saturated Hydraulic Conductivity

Values of saturated hydraulic conductivity (K_s) depth intervals were determined at selected using the constant head method. The K_s values ranged from 1.10cm/day in fragipan to 65.3cm/day in B24t horizon. The second lowest value was obtained between 13-18cm depth, which is probably due to the existance of the plow pan in this region. The variation in K_s in the fragipan corresponded to those of bulk density, the higher the bulk density, the lower K_s. Due to the massive structure at Ap2 horizon, the K_s was significantly low and was 3.55cm/day. The magnitude of the K_s increased in the B1, B21t, and B22t horizon which is possibly due to the blocky structure of these horizons. A vast variation in K_s was found in the B23t & BX1 and BX2 horizons which are in the range of fragipan.

Unsaturated Hydraulic Conductivity

Unsatruated hydraulic conductivity (K) was determined as a function of soil depth, hydraulic gradient, and change in moisture content in-situ. As Richard, et al. 1957 mentioned the field method is generally more reliable than the laboratory method in determining K values. The "zero flux method" (equation 3 and 4) were used to determine K. The high values were obtained for unsaturated hydraulic conductivity in all selected depth at the beginning of the drainage cycle, the values become samller as the drying process continued. The data in Fig. 15 through 19 represent the regressions between unsaturated hydraulic conductivity and soil moisture content for the selected depth intervals. Due to the importance

of the moisture near the soil surface, the K values from 1 to 15cm depth were determined separtely and were plotted as a function of soil water content. The data in Fig. 19 indicate an average between K values and volumetric water content, θ_v from 1 to 15cm depth. The maximum slope of the regression curves were obtained in the fragipan and a relatively high slope was found between 10 to 15cm depth, which is due to the presence of the plow pan. The slopes range from 53.98 at Ap2 to 131.35 at B23t ǂBX1. Correlation coefficient, R, ranged from 0.969 to 0.855. The data in Table 6 Appendix A shows the magnitude of the selected parameters which describs the mathematical model for the functional relationships between unsaturated hydraulic conductivity and volumetric soil water content.

A comparison was made of the K_s values obtained using the laboratory method and the theoretical method. In this method the lnk values were plotted as a function of the deficit volumetric water content from the saturation volumetric water content, $(\theta_s - \theta_v)$. The data in Fig. 21 in Appendix B represent the regression curves which describe the functional relationships between unsaturated hydraulic conductivity and $(\theta_{sat.} - \theta_{vol.})$. Theoretical values for K_s were obtained by assuming the volumetric water contents be the same as the volumetric water content at saturation, that is $\theta_s = \theta_v$. By this assumption, the K values are the same as the K_s values and the magnitude of the K_s is the value of the intercept of the regression curve. Data in Table 7, Appendix A represents the values for K_s determined in the laboratory by the constant head method, and the theoretical method obtained from the functional relationships between K and $(\theta_s - \theta_v)$. A significant correlation coefficient of 0.838 was found between these parameters.

Soil Water Diffusivity

Soil water diffusivity for the evaporation stage II was calculated form data shown in Fig. 23. Cummulative evaporation, E for the drying period from July 1 through July 7 are presented. The data were plotted as a function of square root of time, in days. This method was applied by Black, 1969. The coefficient, A in equation 9 was determined to be $0.4cm/(day)^{-\frac{1}{2}}$. Weighted mean diffusivity was calculated using equation 8 with the assumptions that θ_o, which is the water content at the boundary (x=o) is equal to zero, and θ_i to be the magnitude of the water content at the beginning of the stage II. The value for θ_i was 0.343 cm^3/cm^3. Consequently the values for $(\theta_i - \theta_o)$ was found to be 0.343 cm^3/cm^3. The data in Fig. 22 and 23 represent the processes in order to calculate soil water diffusivity.

Soil Reflectivity

The relationships between soil moisture content and reflectivity at 1.5 and 6.0 GH_z are shown in Fig. 24 through 32 in Appendix B. In three drying cycles, relationships between reflectivity and soil moisture content were interpreted to have two distinct phases. Phase I, occurs where the reflectivity values chang slightly along with corresponding decrease in soil water content at the surface. In phase II the reflectivity values decreased sharply. At 0-5cm depth, soil water content decreased from 0.400 to $0.060cm^3/cm^3$. The reflectivity at the same time decreased from 0.60 to 0.12 at 1.5 GH_z and from 0.20 to 0.02 at 6.0 GH_z. Linear regression analyses were performed to relate the coefficient of reflectivity, r, with the volumetric soil water content for both phases at the soil surface. It is to be noted that the first drainage cycle

was not completed, therfore the data on Fig. 24 and 25 show the relationships between soil moisture content and soil reflectivity during the phase I. The data in Table 8 in Appendix A, represent the slopes, correlation coefficients, and intercepts for two frequencies 1.5 and 6.0 GH_z. The data shown in Fig. 32 indicate that, the relationship between reflectivity and soil moisture content is linear in one phase if the volumetric water content is obtained by gravimetric sampling rather than using the data from moisture retention curve.

The relationships between soil reflectivity and the other soil moisture parameters will be discussed after the data are analyzed.

LITERATURE CITED

1. Arya, L. M., Black, G. R., and Farrell, D. A. 1975. A field study of Soil Water Depletion patterns in presence of growing soybean roots, SSSA, Vol. 39, no. 3.

2. Choudhury, B. J., Schmugge, T. J., Newton, R. N. and Chang, A. 1978. Effect of surface roughness on the microwave emission from soils, NASA, Technical memorandum 79606.

3. Crank, J. 1956. The mathematics of diffusion, Oxford press, London: pp. 31.

4. McCall, E. M. 1977. Analysis of radiative transfer model for the prediction of microwave emission and soil moisture, Department of Electrical Engineering, Univeristy of Arkansas, Fayetteville pp. 1-3.

5. Meylan, P., Morzier, C., Musy, A. 1981. Determination of changes in the hydrologic and thermal profiles of soil by simulation and remote sensing, Agristars.

6. Waite, W. P., Cook, K. R., Bryan, B. B. 1973. Broad spectrum microwave systems for remotely measuring soil moisture content, WRRC, University of Arkansas, Pub. #18.

7. Wang, J. R. 1979. The dielectric properties of soil water mixtures at microwave frequencies, Technical Memorandum, 80597.

APPENDIX A

Table 1. Morphological description of Captina silt loam.

Horizon	Depth (cm)	Descriptions
Ap	0-18	Dark grayish brown (10 Y/R 4/2) silt loam; weak find granular structure; friable; few fine roots; clear smooth boundary.
Ap2	18-29	Brown (10 1/R 5/3) silt loam with few fine faint yellowish brown (10 1/R 5/4) mottles; massive structure; friable; common fine roots; numerous dark grayish brown (10 1/R 4/2) worm and root channels; many discontinuous pores (1-4 mm dia.); 1% coarse fragments; clear wavy boundary.
B1	29-45	Yellowish brown (10 1/R 5/4) silt loam; weak subangular blocky structure; friable; few fine roots; numerous dark brown (10 1/R 4/3) worm and root channels; few pores (1-6 mm dia.); clear smooth boundary.
B21t	45-61	Yellowish brown (10 1/R 5/6) silt loam; medium subangular blocky structure; friable; thin patchy yellowish brown (10 1/R 4/5) clay films on vertical faces of peds; few fine roots; few pores (1-1.5 mm dia.); clear wavy boundary.
B22t	61-72	Yellowish brown (10 1/R 5/4) silty clay loam; moderate medium subangular blocky structure; film; thin patchy yellowish brown (10 1/R 5/4) clay films on vertical faces of peds; few fine roots; a few dark grayish brown (10 1/R 4/2) coatings in root channels; few fine pores; 5% coarse fragments; clear irregular boundary.
B23t & B&1	71-102	The B23t component (60%) consists of red (2.5 1/R 5/6)silty clay loam; moderate medium subangular blocky structure; firm; thin patchy red (2.5 1/R 5/6) clay films on vertical and horizontal ped faces; no roots; many fine black (N 2/) FeMn stains; clear wavy boundary.

Table 1. Morphological description of Captina silt loam.

Horizon	Depth (cm)	Descriptions
		The Bx1 component (40%) consits of red (2.5 1/R 4/6) heavy silt loam with many common medium distinct fine permanent pinkish gray (7.5 1/R 6.2) and yellowish brown (10 1/R 5/6) mottles; weak medium prismatic structure; very firm, slightly brittle; common pores (0.5-2 mm dia.); many coarse distinct black (N2/) FeMn stains on prism faces; clear wavy boundary.
Bx2	102-117	Red (2.5 1/R 5/6) silty clay loam with common fine prominent dark yellowish brown (10 1/R 4/6) and some yellowish brown (10 1/R 5/4) mottles; prismatic structure; firm and brittle; common pores (0.5-2 mm dia.); many firm black (N 2/) FeMm stains on prism faces, 10% coarse fragments; clear wavy boundary.
B24t	117-140	Red (2.5 1/R 4/4) silty clay loam with many coarse medium distinct pale brown (10 1/R 6/3) and yellowish brown (10 1/R 5/4), common coarse distinct pinksih gray (7.5 1/R 6/2), and a few fine prominent strong brown (7.5 1/R 5/6) mottles; moderate coarse subangular blocky structure; firm reddish brown (2.5, 1/R 4/4) and dark yellowish brown (10 1/R 4/4) clay films; vertical gray (N6/) seams; common fine black (N2/) FeMn stains and nodules; gradual wavy boundary.

Table 2. Selected physical properties of the Captina soil.

Depth Interval	Bulk Density	Particle Density	Sand	Silt	Clay	K_{Sat}	Total Porosity
(cm)	(g/cm^3)	(g/cm^3)	---------%----------			cm/day	(cm^3/cm^3)
0-5	1.27	2.49	25.5	64.1	10.4	6.19	0.490
13-18	1.41	2.56	28.6	61.3	10.1	3.55	0.449
28-33	1.39	2.62	22.9	63.3	13.8	32.23	0.469
43-48	1.39	2.60	21.0	62.9	16.1	43.87	0.465
58-63	1.50	2.62	18.5	59.2	22.3	21.05	0.427
73-78	1.58	2.61	17.3	55.2	27.5	26.38	0.395
88-93	1.64	2.62	18.0	52.3	29.7	1.10	0.374
103-108	1.54	2.62	18.8	57.2	24.0	16.01	0.412
118-123	1.53	2.63	39.6	35.1	25.3	3.82	0.418
133-138	--	2.62	18.3	56.7	25.0	65.30	--

Table 3. Particle size distribution of Captina silt loam.

Depth Interval (cm)	Percentage Composition											
	VCS	CS	MS	FS	VFS	Total Sand	CSi	MSi	FSi	Total Silt	Total Clay	Textural Classification
0-5	0.7	1.1	2.3	8.7	12.6	25.5	35.7	22.5	6.0	64.1	10.4	SIL
11-18	1.4	1.8	2.6	8.9	13.8	28.6	32.4	22.6	6.3	61.3	10.1	SIL
28-33	0.9	1.4	2.1	7.4	11.1	22.9	32.1	24.5	6.7	63.3	13.8	SIL
43-48	0.6	1.1	2.0	6.8	10.5	21.0	31.9	24.7	6.3	62.9	16.1	SIL
58-63	0.4	0.7	1.6	6.1	9.7	18.5	29.3	21.8	8.1	59.2	22.3	SIL
73-78	0.2	0.4	1.3	5.9	9.5	17.3	29.2	17.6	8.4	55.2	27.5	SIL
88-93	0.4	0.5	1.4	6.1	9.6	18.0	27.9	18.4	6.0	52.3	29.7	SICL
103-108	0.4	0.6	1.4	6.3	10.1	18.8	29.9	17.7	9.6	57.2	24.0	SIL
118-123	0.8	0.8	1.6	6.4	29.9	39.6	11.7	15.7	7.8	35.1	25.3	L
133-138	0.7	0.7	1.3	5.7	9.9	18.3	27.6	17.5	11.6	56.7	25.0	SIL

Table 4 . Regression coefficients (R^2), intercepts (A), and slopes(B) for the semilog transformation of the soil moisture retention data

Soil Horizon	R^2	A	B
Ap	0.980	8.09 ± 0.46	-28.85 ± 1.37
B_1	0.984	7.38 ± 0.37	-30.28 ± 1.24
B21t	0.981	9.99 ± 0.53	-35.85 ± 1.62
B22t	0.981	10.02 ± 0.53	-35.98 ± 1.62
B23t	0.971	15.12 ± 0.96	-48.32 ± 2.77
B x 1	0.971	15.12 ± 0.96	-48.32 ± 2.77
B x 2	0.967	18.19 ± 1.21	-59.58 ± 3.61
B24t	0.873	23.14 ± 3.51	-73.42 ± 9.32

Table 5. Values of the evaporation Rate (flux) at 1cm depth and drainage rate (flux) across 122cm depth during the second drainage cycle.

Date (day)	Evaporation Rate cm/day	Drainage Rate cm/day
7-1-80	0.420	2.560
7-2-80	0.341	0.712
7-3-80	0.472	0.268
7-4-80	0.318	0.168
7-5-80	0.242	0.106
7-6-80	0.203	0.093
7-7-80	0.158	0.051
7-8-80	[1/]	0.031
7-9-80	--	0.056
7-11-80	--	0.025
7-14-80	--	0.019
7-17-80	--	0.006

[1/] We were not able to calculate flux of water at the soil surface because the microtensiometers did not operate at that degree of dryness.

Table 6. Statistical parameters of the relationship between K and θ_v.

Captina Silt Loam

Depth Interval (cm)	(b) Intercept (cm/day)	Slope	R
15-31	2.56×10^{-9}	53.98	0.956
31-46	8.39×10^{-11}	66.34	0.931
46-61	5.18×10^{-13}	79.29	0.910
61-76	1.93×10^{-16}	96.00	0.936
76-91	8.50×10^{-23}	131.35	0.911
91-107	7.17×10^{-18}	101.93	0.945
107-122	1.25×10^{-18}	107.62	0.855

Table 7. Comparison between two methods of determining saturated hydraulic conductivity.

Depth Interval (cm)	Saturated Hydraulic Conductivity, $K_{sat.}$ cm/day	
	Calculated	Experimental
15-31	24.40	17.89
31-46	61.00	38.05
46-61	57.00	22.96
61-76	12.70	23.71
76-91	8.60	13.74
91-107	3.60	8.56
107-122	2.78	9.91

Table 8. Correlation coefficients, slopes and intercepts of the regression equations of two phases from the three drainage cycles.

Drainage Cycle	Phase	Frequency 1.5 GH_z R	m	b	6.0 GH_z R	m	b
1	1	0.597	0.69	0.282	0.432	0.44	0.170
1	1/	--	--	--	--	--	--
2	1	0.543	0.59	0.330	0.153	0.07	0.132
2	2	0.952	6.77	-1.856	0.911	5.69	-1.730
3	1	0.644	0.73	0.282	0.211	0.103	0.130
3	2	0.933	9.18	-2.660	0.925	5.53	-1.690
2&3	1	0.633	0.795	0.255	0.212	0.106	0.123
2&3	2	0.936	7.110	-1.970	0.932	5.31	-1.610

1/ Not a complete cycle.

Table 9. Reflectivity measurements from first drainage cycle, June 18 through June 22, 1980.

Date	Time, hr.	Cumulative Time, hr.	Reflectives			
			Frequency 1.5 GH_2	Frequency 6.0 GH_2	Ψ_m -cm	$\bar{\Theta}_v$ cm^3/cm^3
6-18-80	0745	000	0.556	0.398	6.5	0.435
"	1010	002	0.575	0.331	20	0.415
"	1200	004	0.549	0.331	30	0.410
"	1410	006	0.549	0.376	48	0.403
"	1615	008	0.537	0.347	53	0.397
"	1750	010	0.616	0.323	60	0.395
"	2005	012	0.556	0.367	61	0.394
6-19-80	0915	025	0.562	0.331	55	0.396
"	1100	027	0.562	0.323	69	0.390
"	1235	028	0.537	0.331	79	0.380
"	1405	030	0.530	0.323	103	0.367
"	1615	032	0.569	0.343	126	0.360
"	1800	034	0.525	0.343	136	0.355
6-20-80	1030	050	0.569	0.305	108	0.367
"	1210	052	0.549	0.309	148	0.355
"	1415	054	0.519	0.309	177	0.350
"	1550	056	0.519	0.367	157	0.353
6-21-80	0775	073	0.501	0.389	119	0.363
"	1405	079	0.530	0.316	165	0.352
6-22-80	0835	097	0.507	0.323	146	0.356
"	1400	105	0.478	0.316	247	0.340

Table 10. Reflectivity measurements from second drainage cycle, June 30 through July 21, 1980.

Date	Time, hr.	Cumulative Time, hr.	Reflectivity			
			Frequency 1.5 GH_2	Frequency 6.0 GH_2	Ψ_m -cm	$\bar{\Theta}_v$ cm^3/cm^3
6-30-80	08	000	0.575	0.160	9	0.425
"	12	004	0.575	0.157	24	0.415
"	14	006	0.601	0.168	35	0.407
"	16	008	0.575	0.135	60	0.390
"	18	010	0.549	0.153	80	0.380
7-1-80	08	024	0.531	0.178	86	0.375
"	10	026	0.562	0.170	105	0.370
"	12	028	0.562	0.191	135	0.357
"	14	030	0.513	0.162	195	0.350
"	16	032	0.462	0.151	242	0.340
"	18	034	0.432	0.145	275	0.330
7-2-80	08	048	0.442	0.148	180	0.350
"	11	051	0.422	0.148	289	0.325
"	14	054	0.359	0.098	372	0.320
"	17	057	0.282	0.074	462	0.351
7-3-80	08	072	0.310	0.079	437	0.320
"	14	078	0.232	0.039	531	0.315
"	17	081	0.240	0.029	563	0.312
7-4-80	09	097	0	0	621	0.309
"	14	102	0.221	0.026	611	0.310
7-5-80	14	126	0.226	0.022	662	0.307
7-6-80	14	150	0.197	0.027	675	0.305
7-7-80	14	174	0.195	0.027	673	0.306

Table 11. Reflectivity measurements from third drainage cycle, July 28 through August 7, 1980.

Date	Time hr.	Cumulative Time, hr.	Reflectivity Frequency 1.5 GH_2	Reflectivity Frequency 6.0 GH_2	Ψm -cm	$\bar{\theta}_v$ cm^3/cm^3
7-28-80	08	000	0.569	0.164	12	0.420
"	11	003	0.575	0.182	25	0.417
"	14	006	0.631	0.197	53	0.400
"	17	009	0.556	0.158	84	0.380
7-29-80	08	024	0.562	0.144	83	0.380
"	11	027	0.519	0.178	114	0.368
"	14	030	0.525	0.214*	389	0.325
"	17	033	0.431	0.172	272	0.330
7-30-80	08	048	0.422	0.164	245	0.340
"	14	054	0.272	0.090	464	0.320
7-31-80	08	072	0.263	0.096	433	0.320
"	14	078	0.190	0.028	487	0.315
8-1-80	14	102	0.197	0.019	619	0.310

APPENDIX B

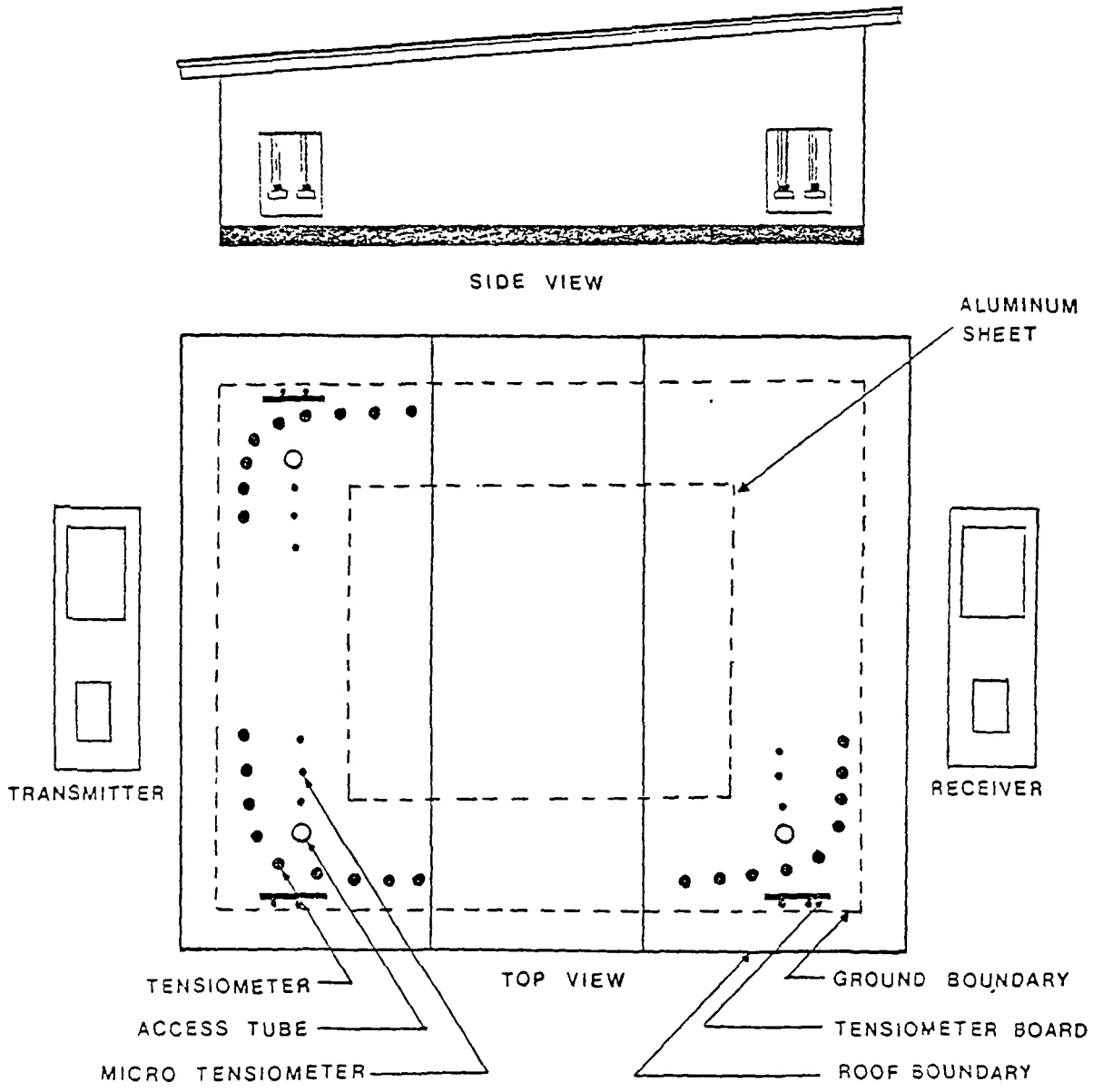

Figure 1. The Schematic diagram for the bare soil experiment of the Summer 1980 at the University of Arkansas.

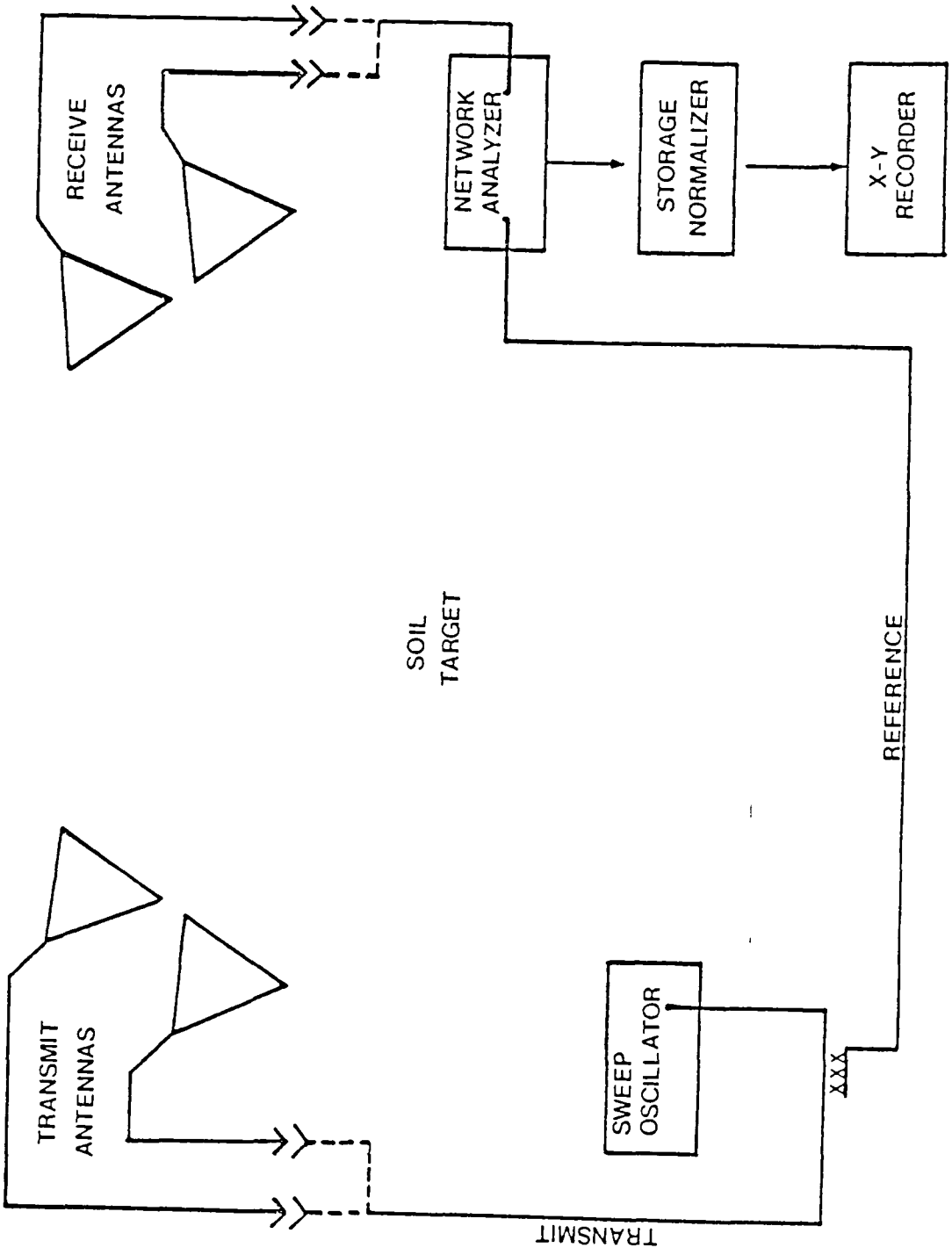

FIGURE 2. BLOCK DIABRAM OF BISTATIC REFLECTOMETER INSTRUMENTATION

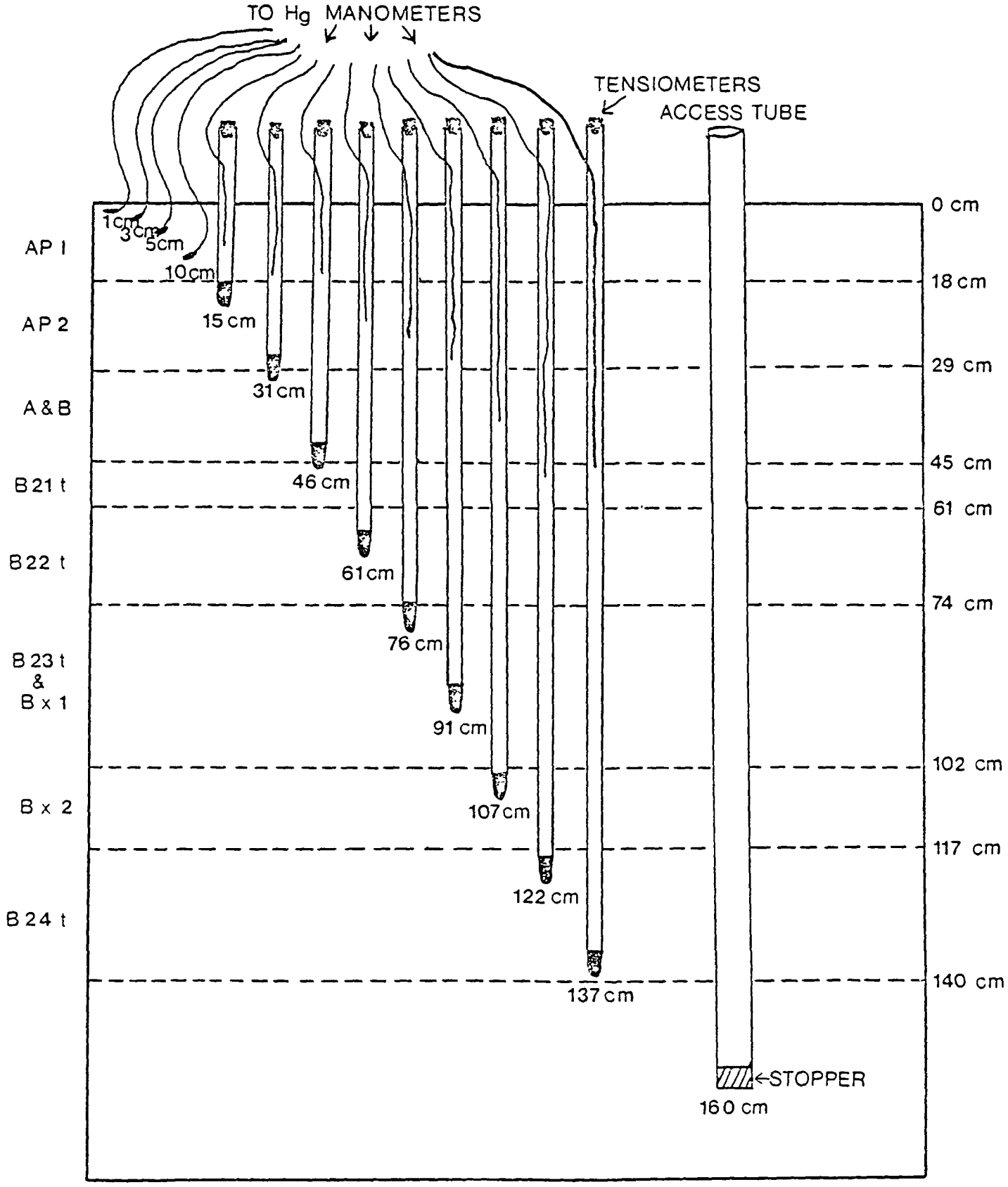

Figure 3. Cross sectional area of each bank

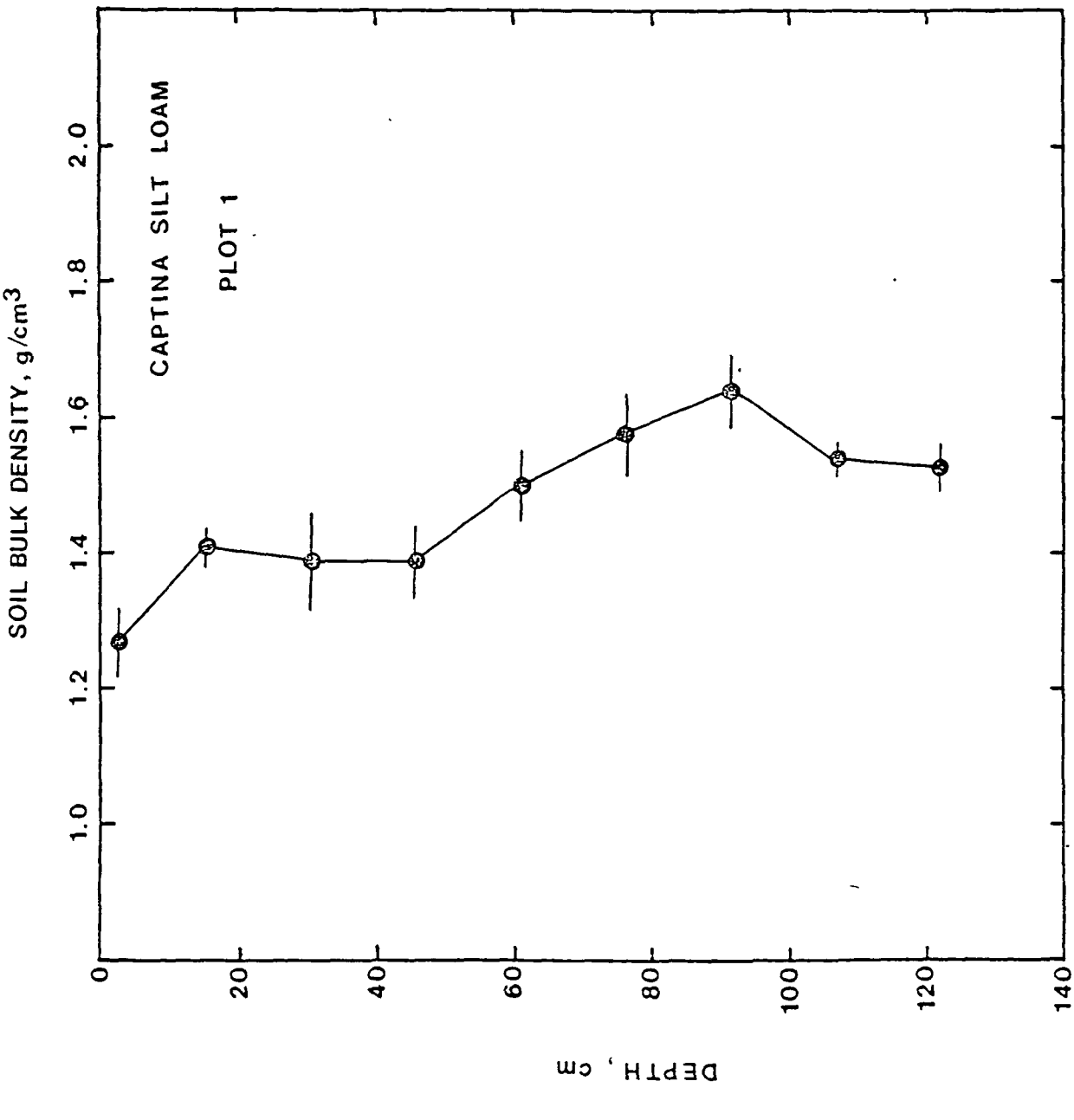

Figure 4. Bulk density of Captina and its standard deviation of the Cores Versus soil depth.

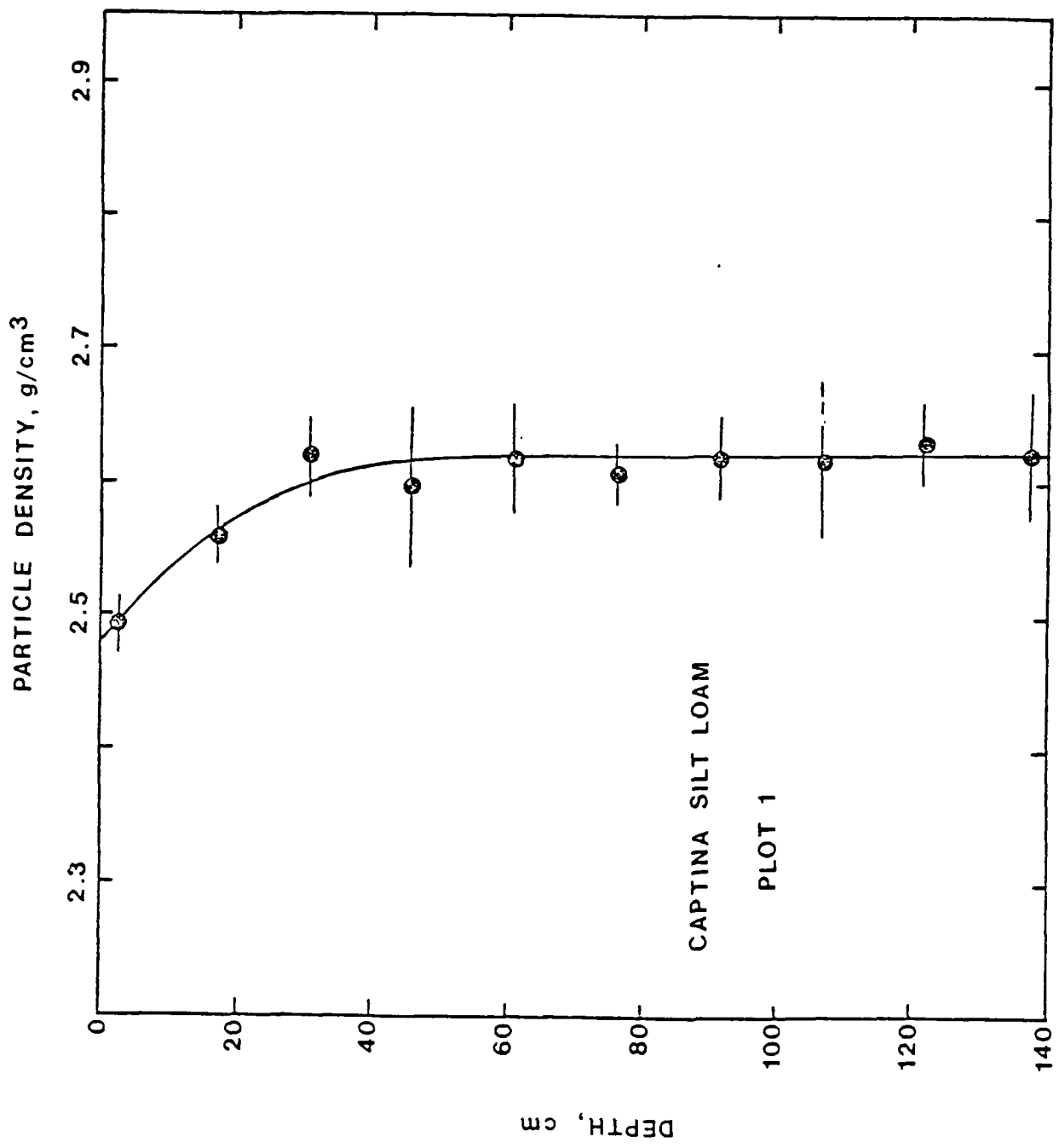

Figure 5. Particle density of the Captina as a function of depth.

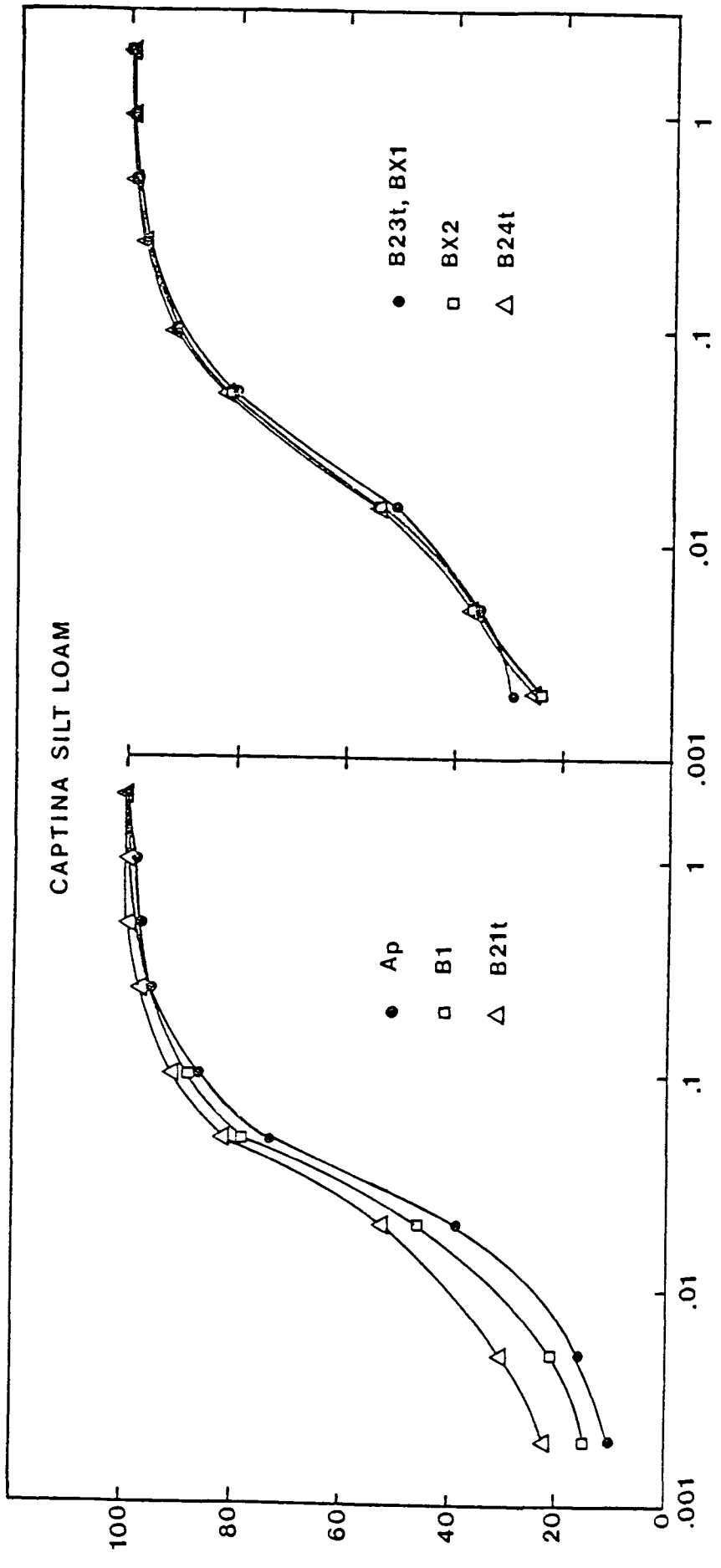

Figure 6. Particle size distribution of the six horizons.

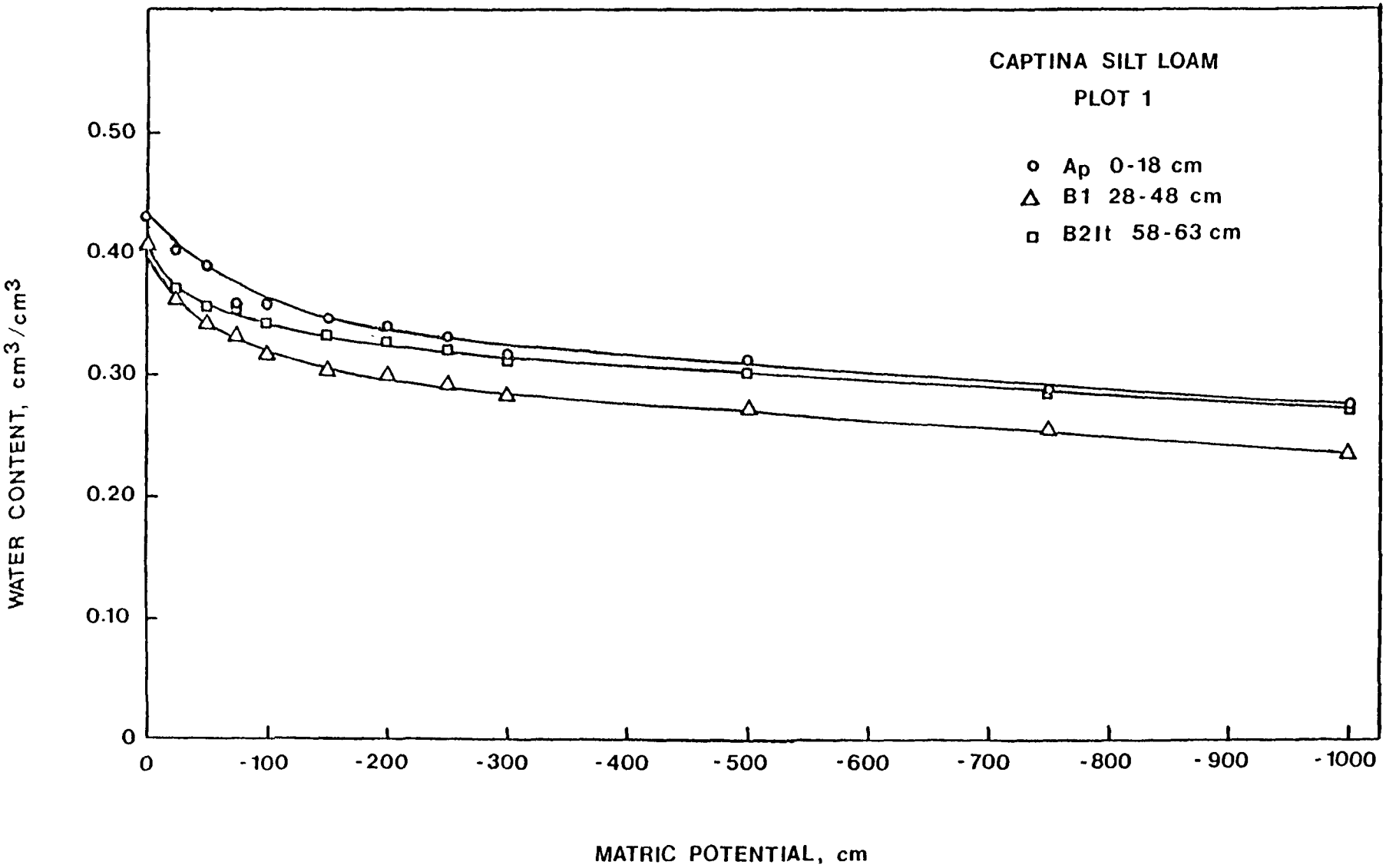

Figure 7. Moisture characteristic curves from the first three upper horizons of Captina soil.

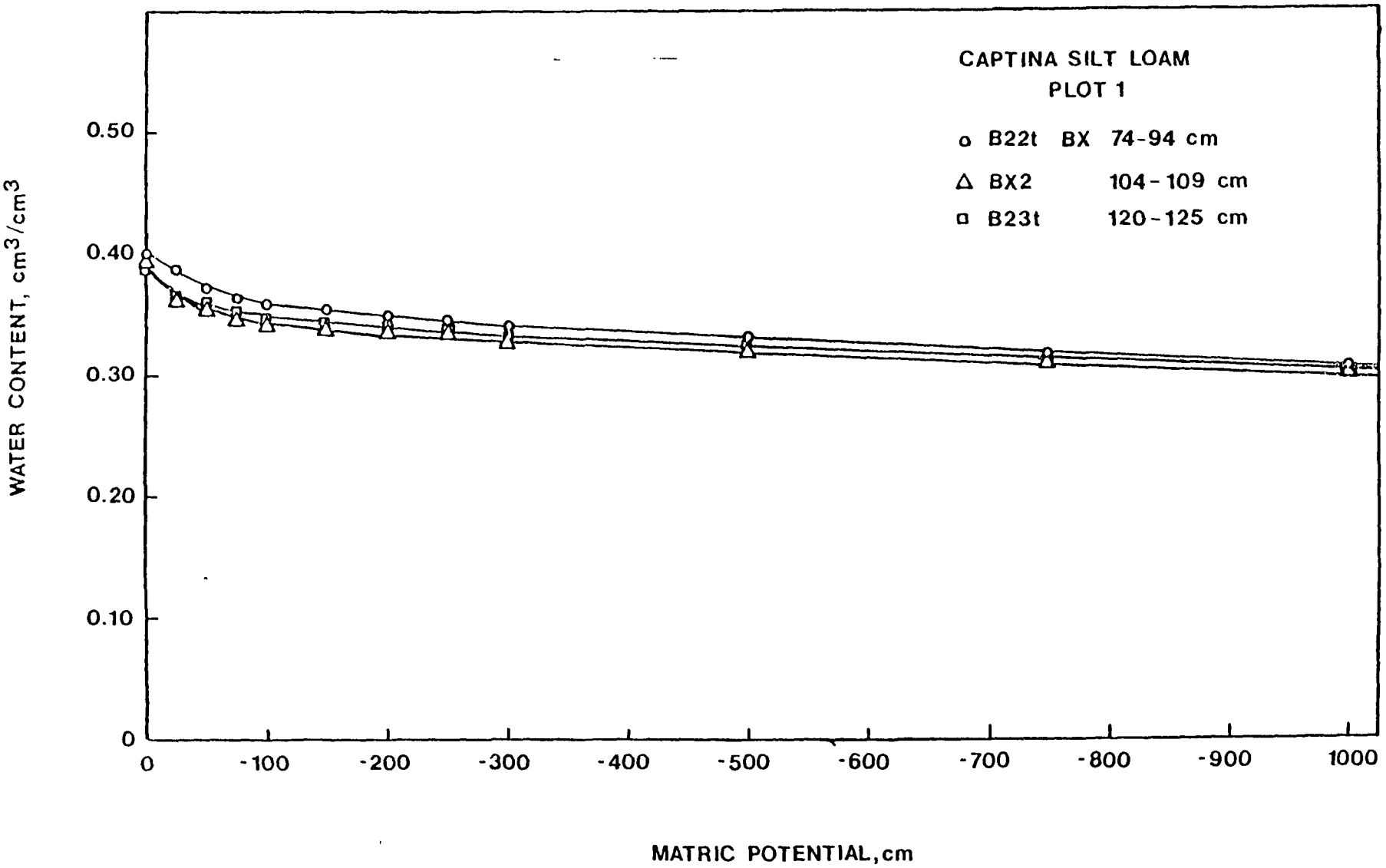

Figure 8. Moisture characteristic curves for the second three lower horizons of Captina soil.

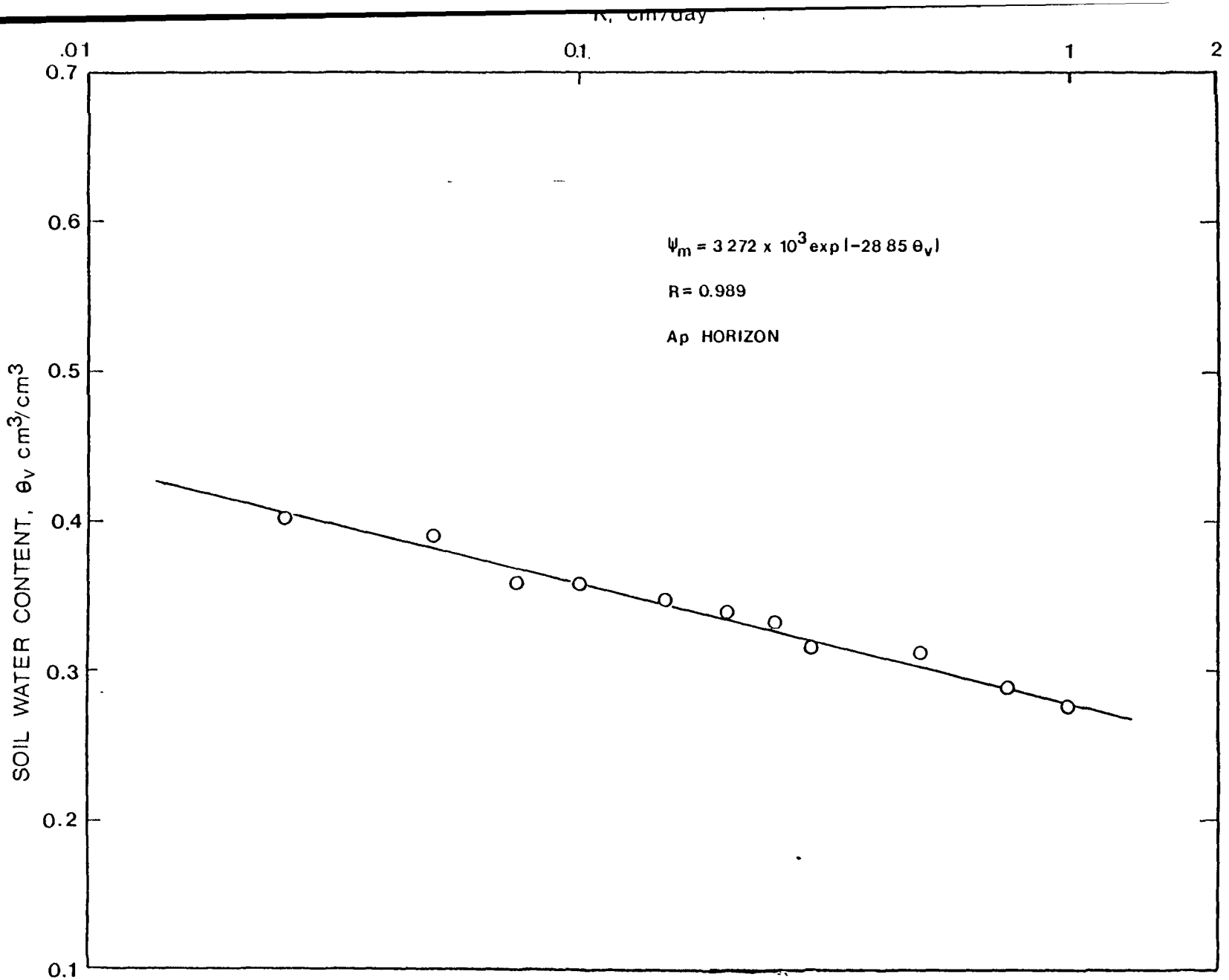

Figure 9 Ap horizon semilog transformation of the soil moisture retention data

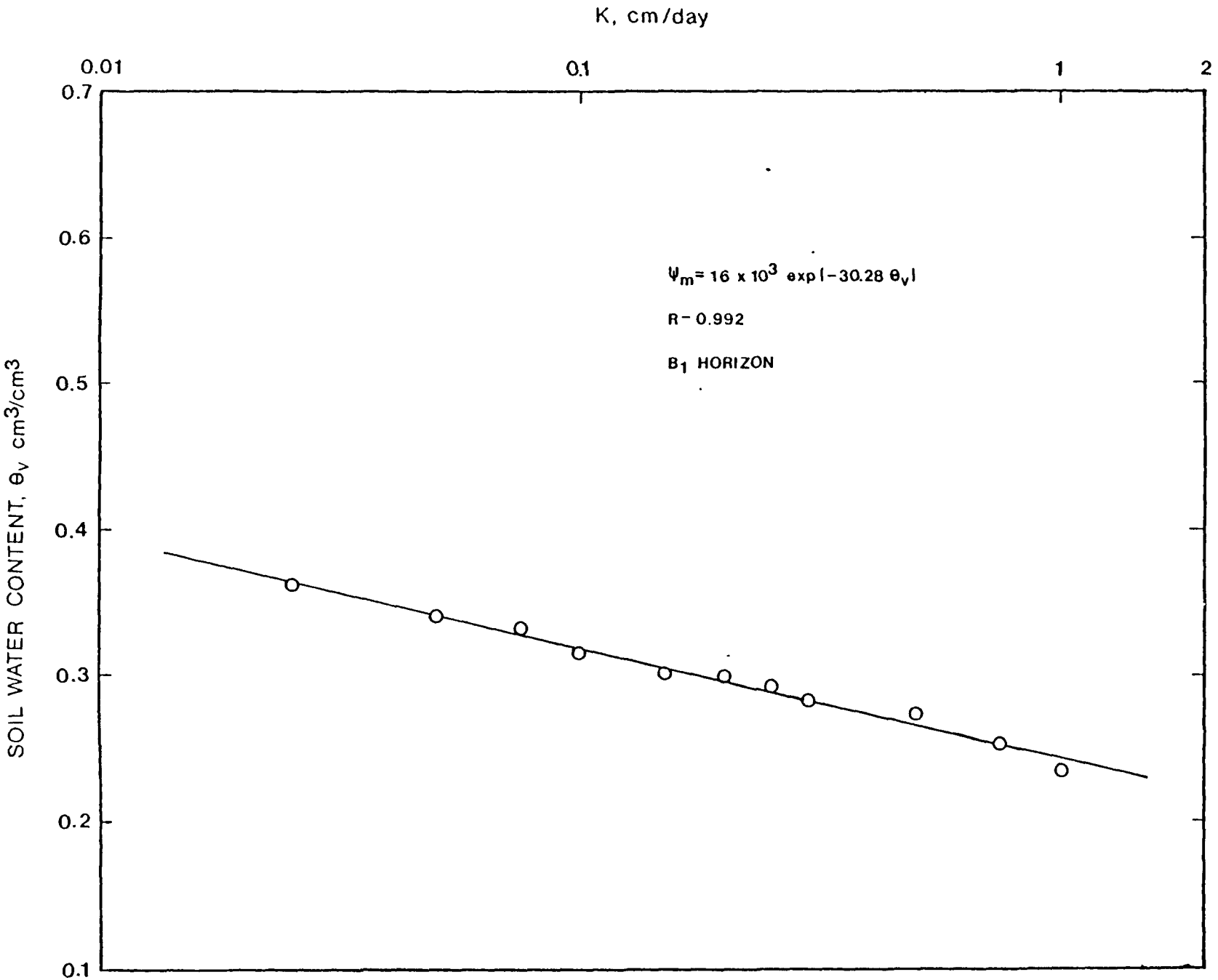

Figure 10 B_1 horizon semilog transformation of the soil moisture retention data

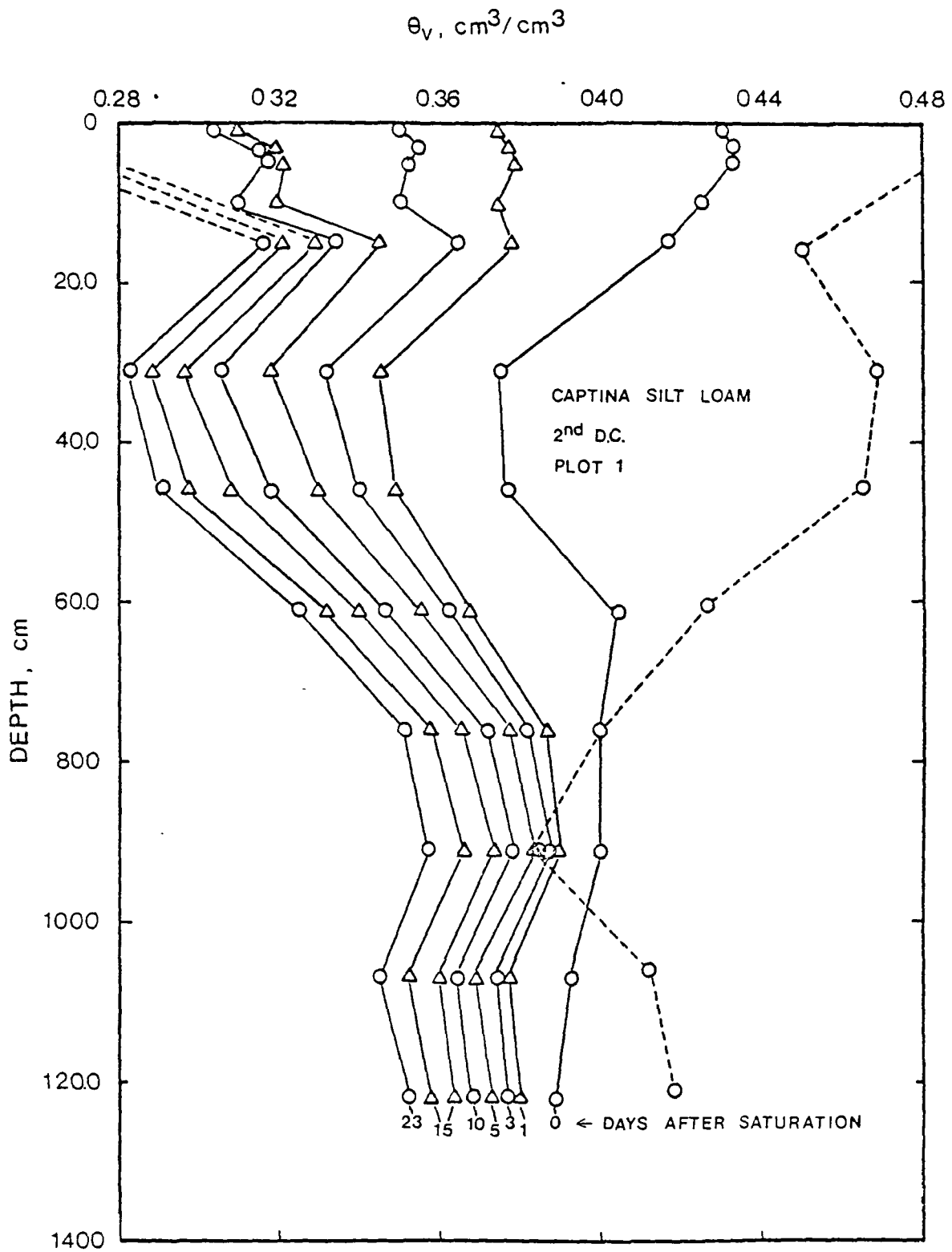

Figure 11. Daily mean volumetric water content as a function of depth at selected days in the second drainage cycle.

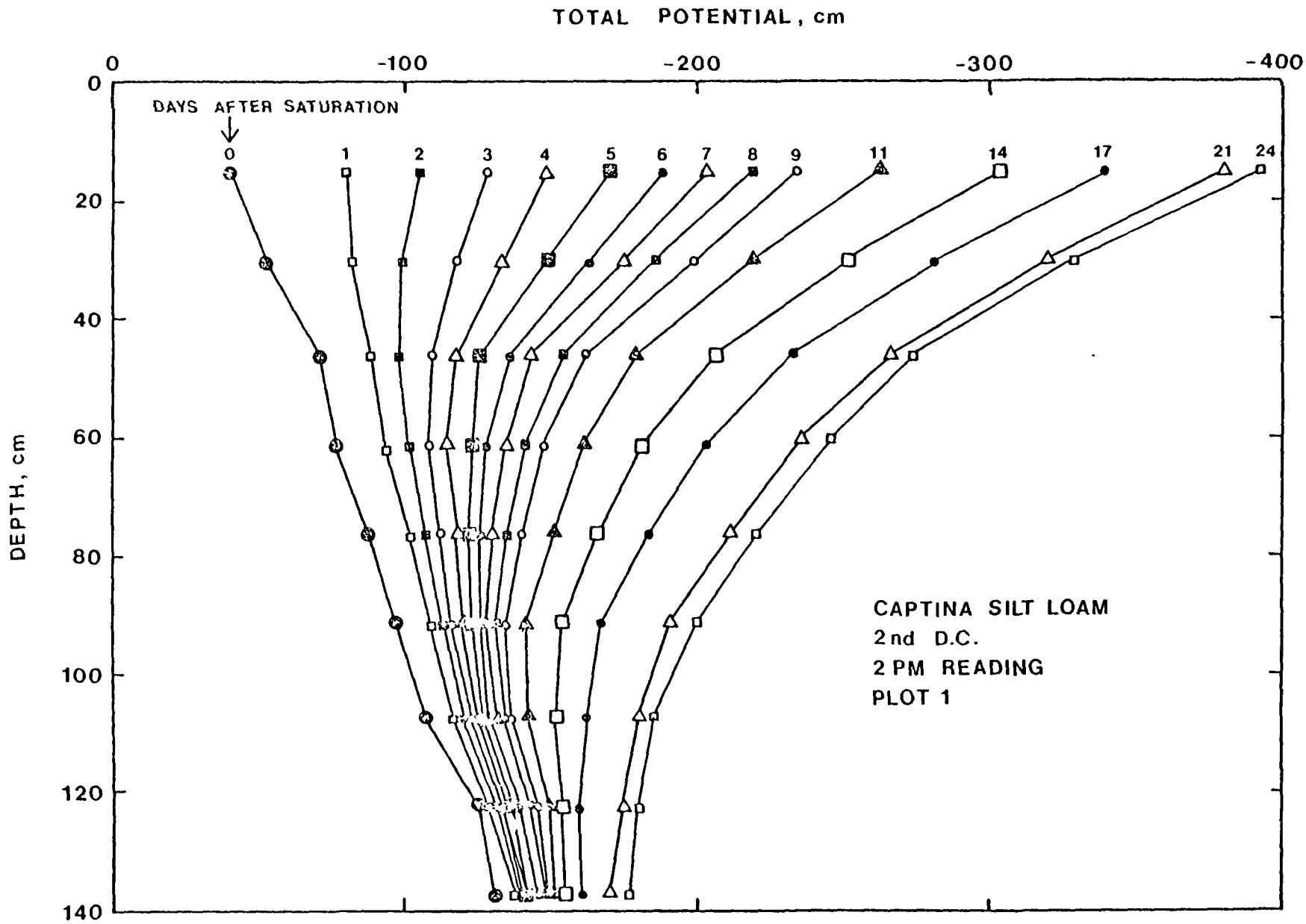

Figure 12. Daily total soil water potential as a function of depth during the second drainage cycle.

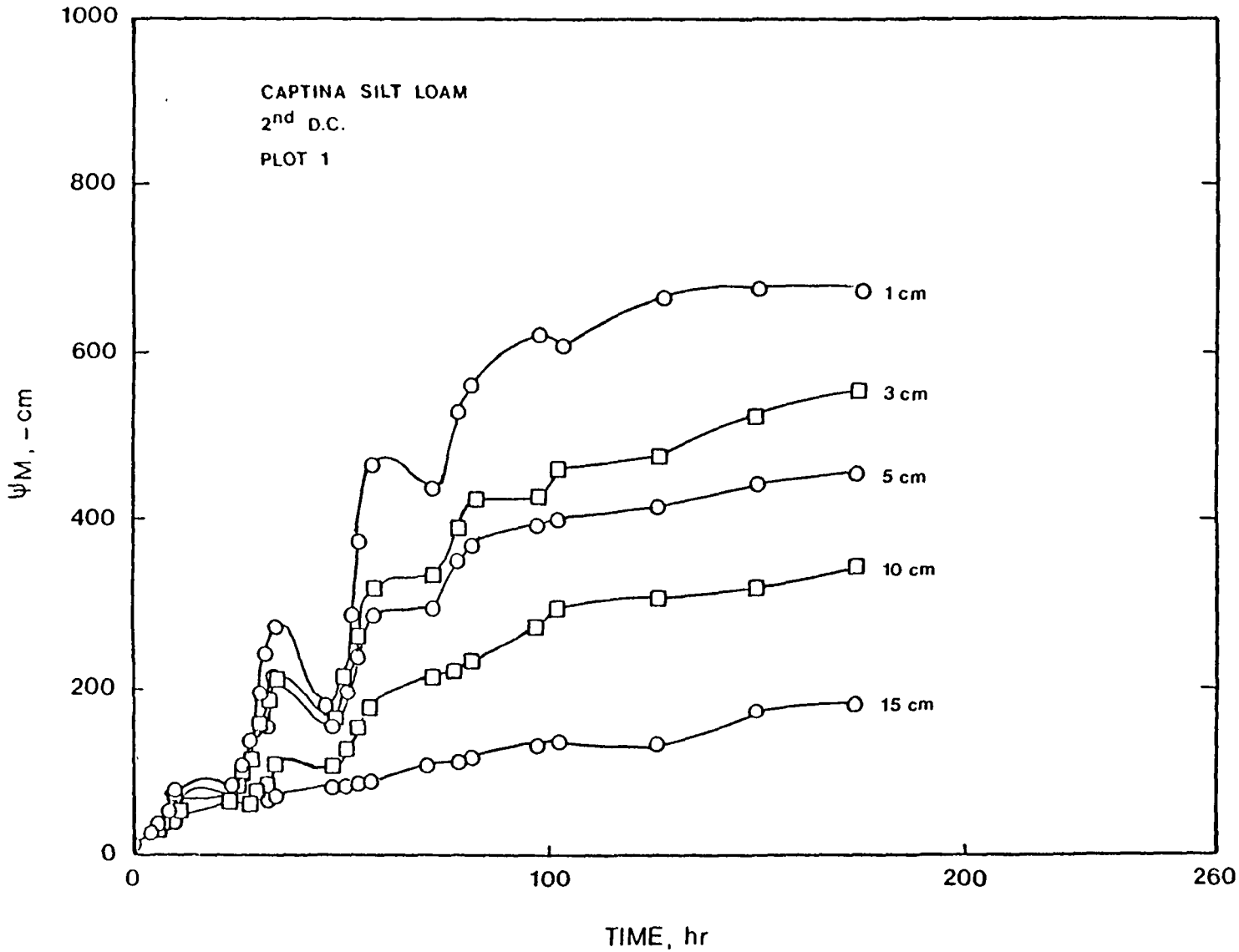

Figure 13. Diural variation in soil matric potential at various depth during the second drainage cycle.

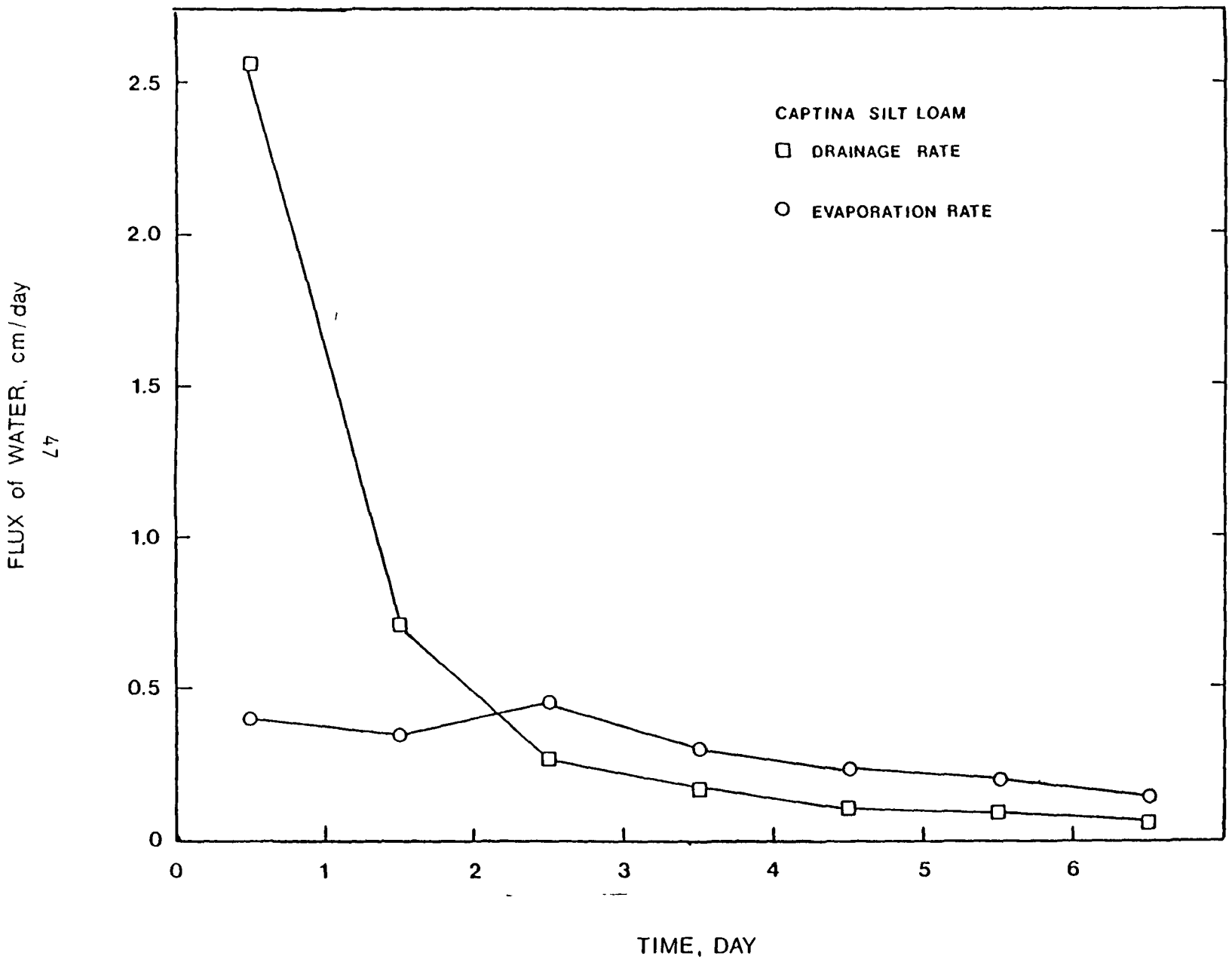

Figure 14. Comparison between average drainage rate and average evaporation rate during the 2nd drainage cycle.

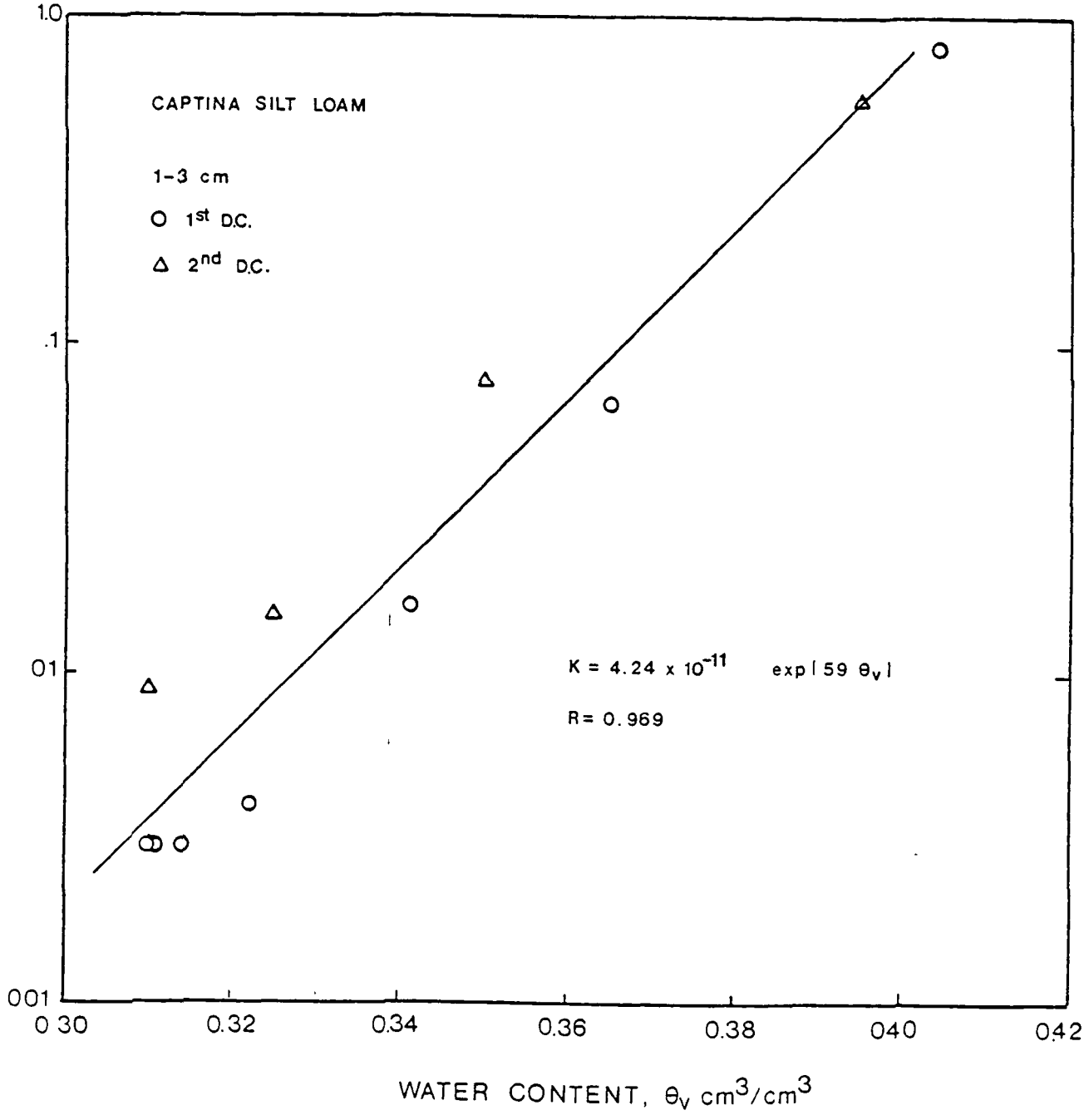

Figure 15. Hydraulic conductivity as a function of soil water content, θ_r, at 1-3 cm depth interval.

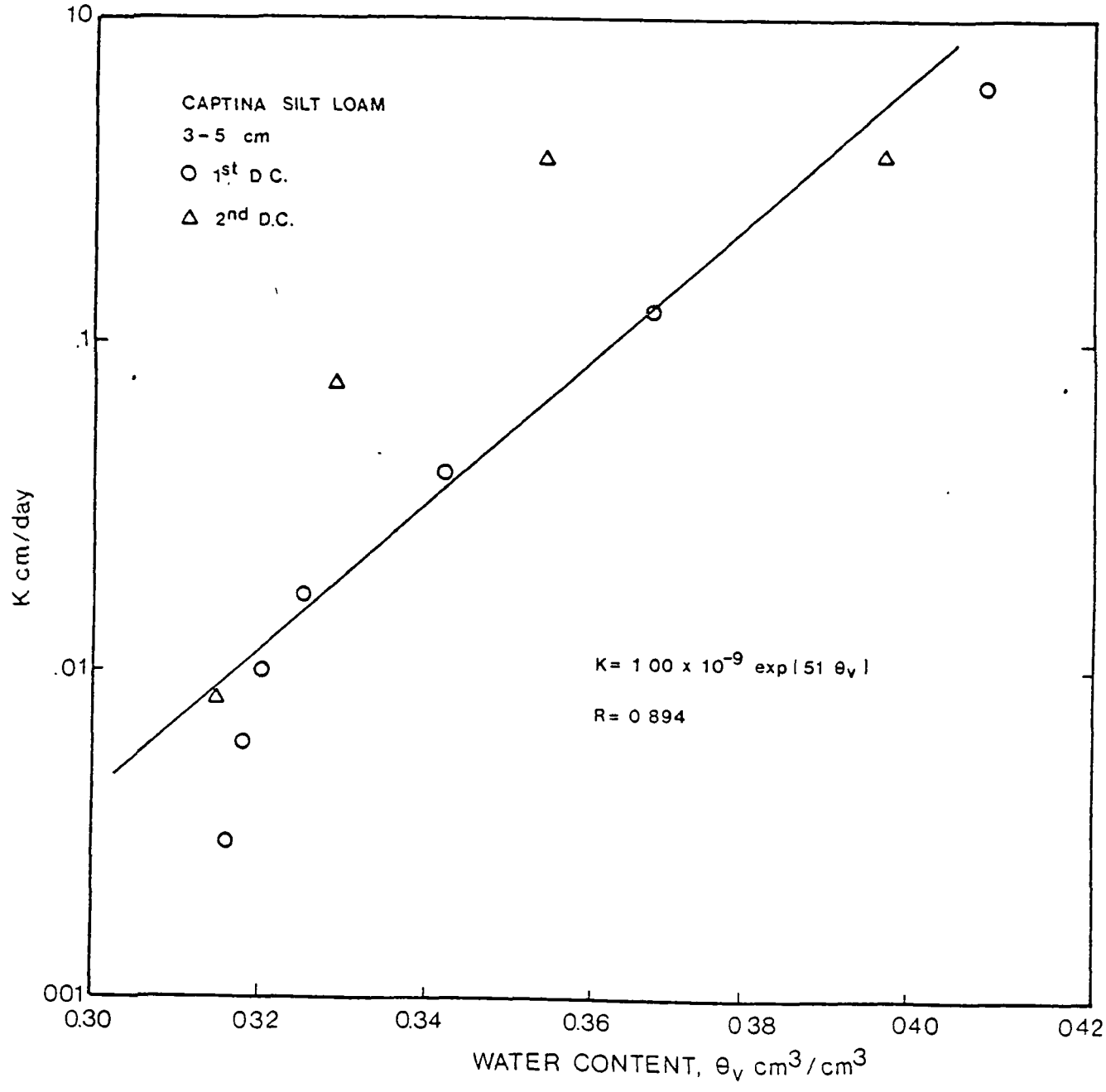

Figure 16. Hydraulic conductivity as a function of soil water content at 3-5 cm depth interval.

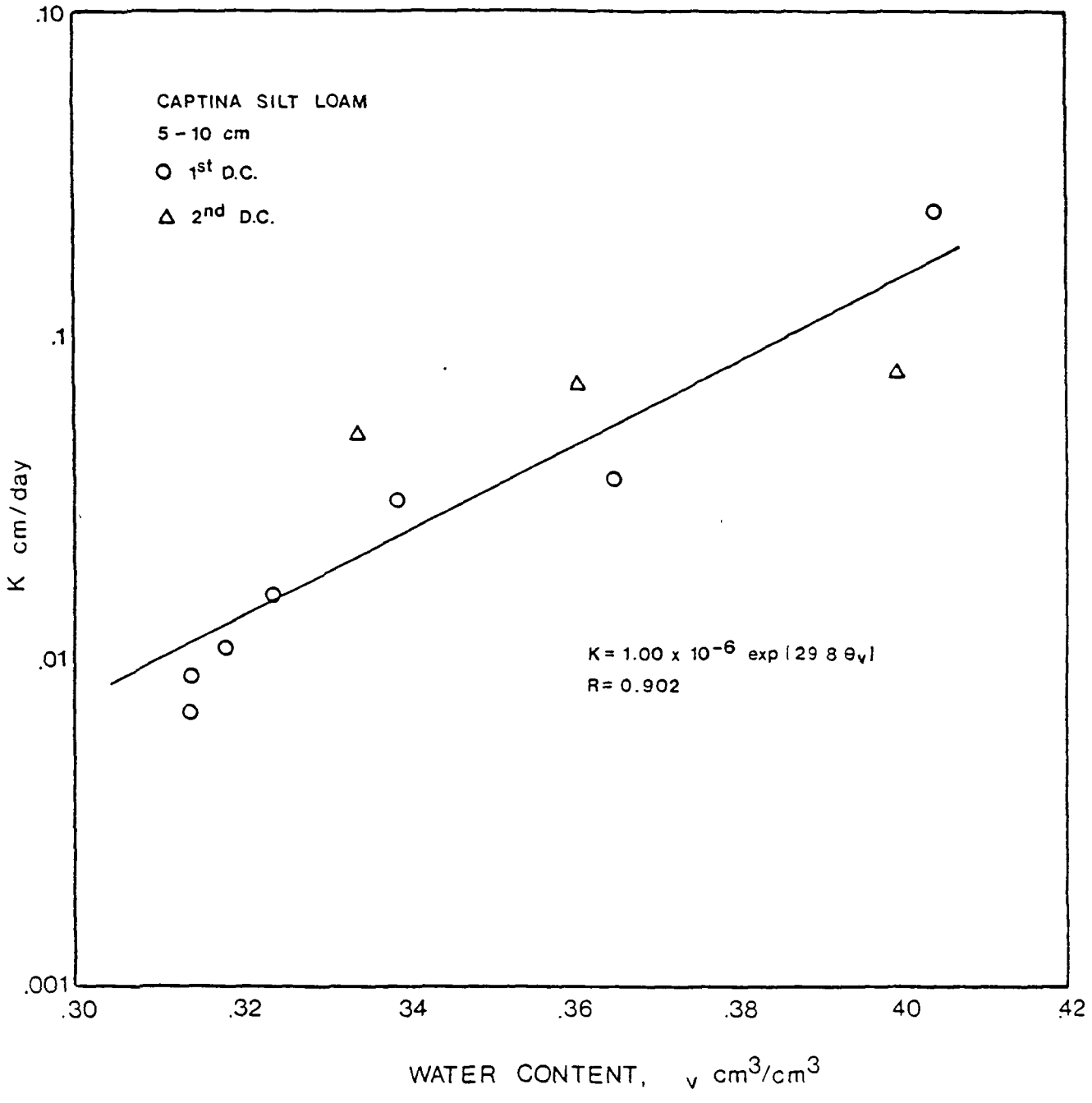

Figure 17. Hydraulic conductivity as a function of soil water content at 5-10 cm depth interval.

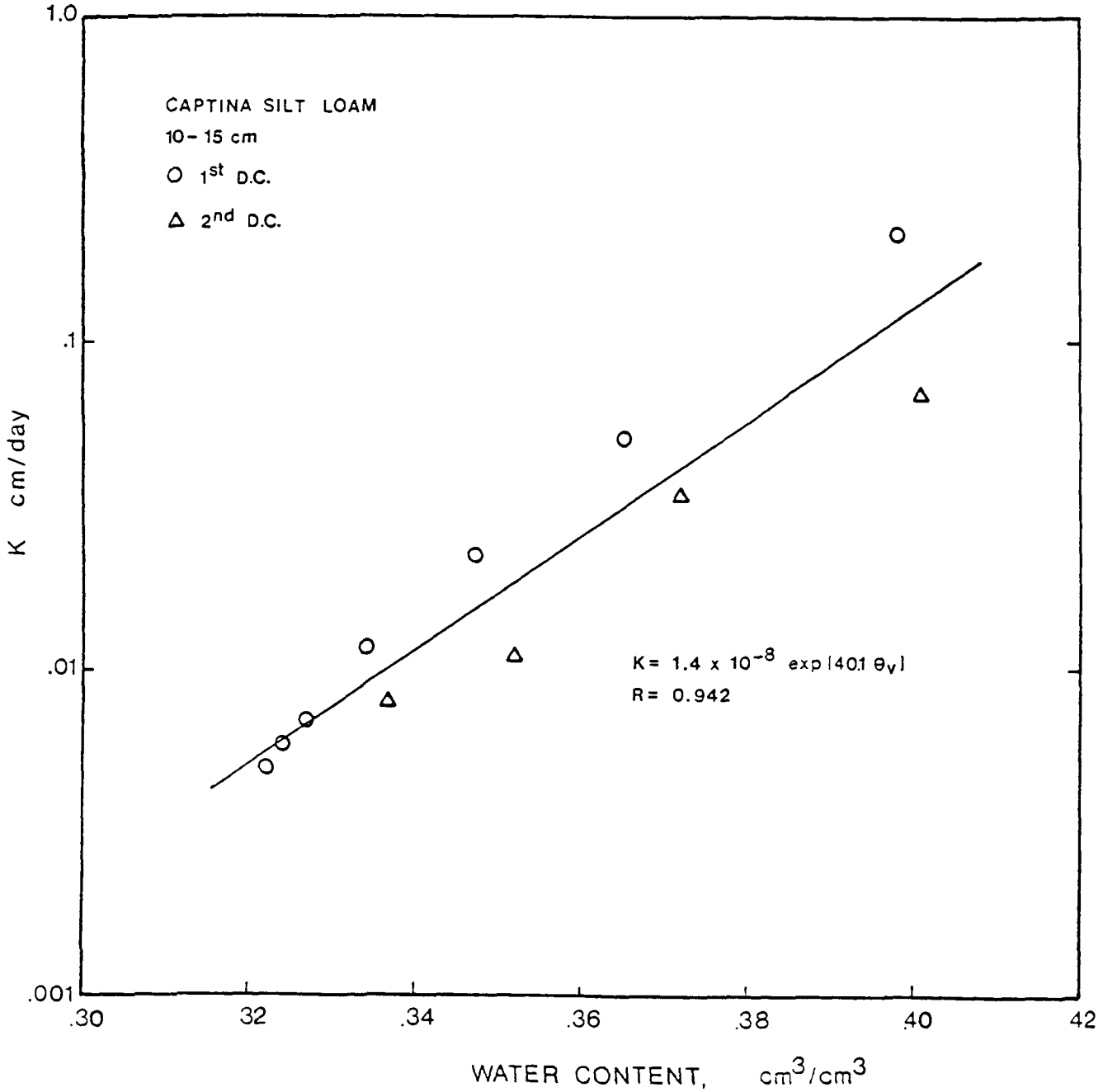

Figure 18. Hydraulic conductivity as a function of soil water content at 10-15 cm depth interval.

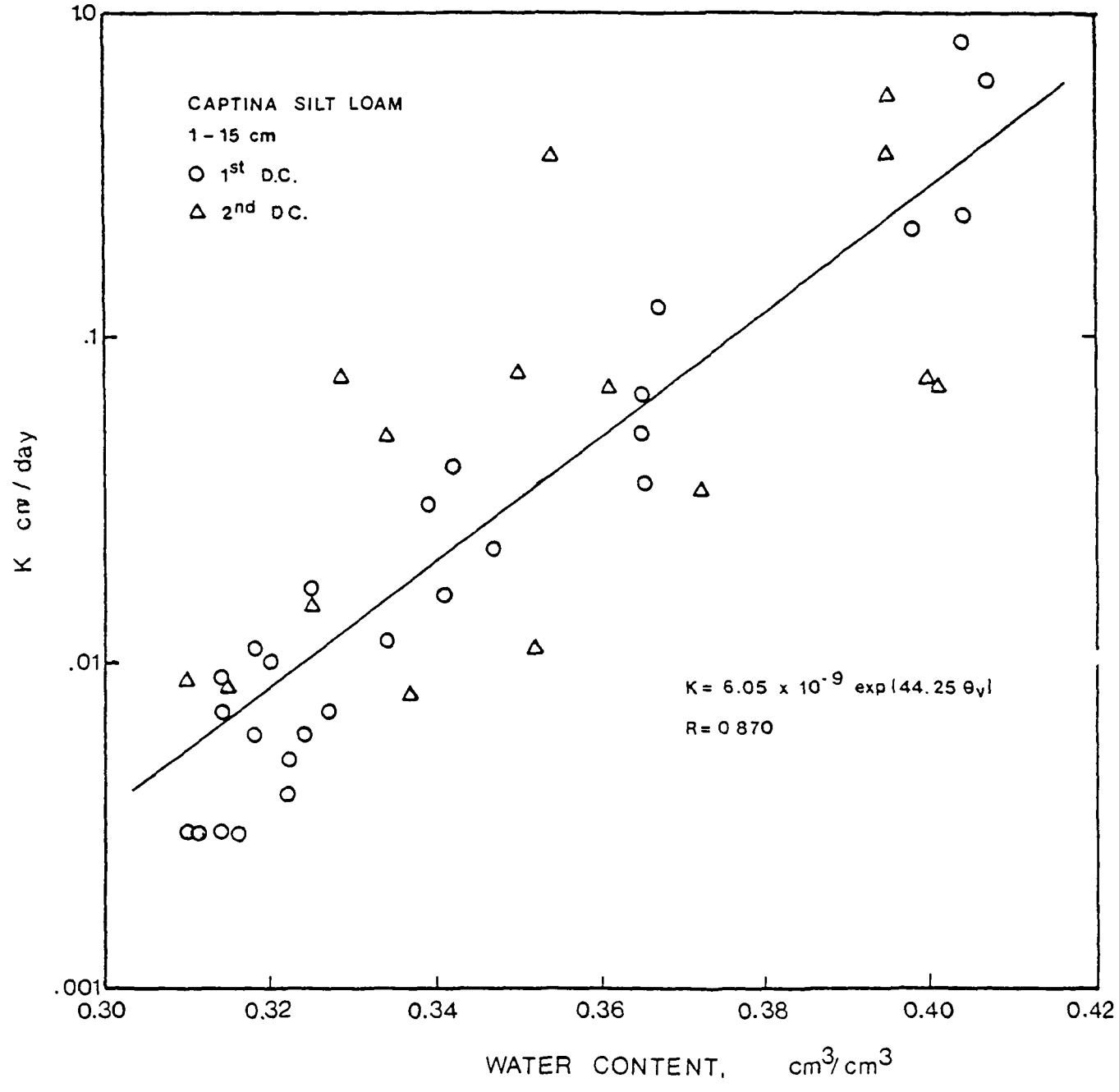

Figure 19. Hydraulic conductivity as a function of soil water content at 1-15 cm depth interval.

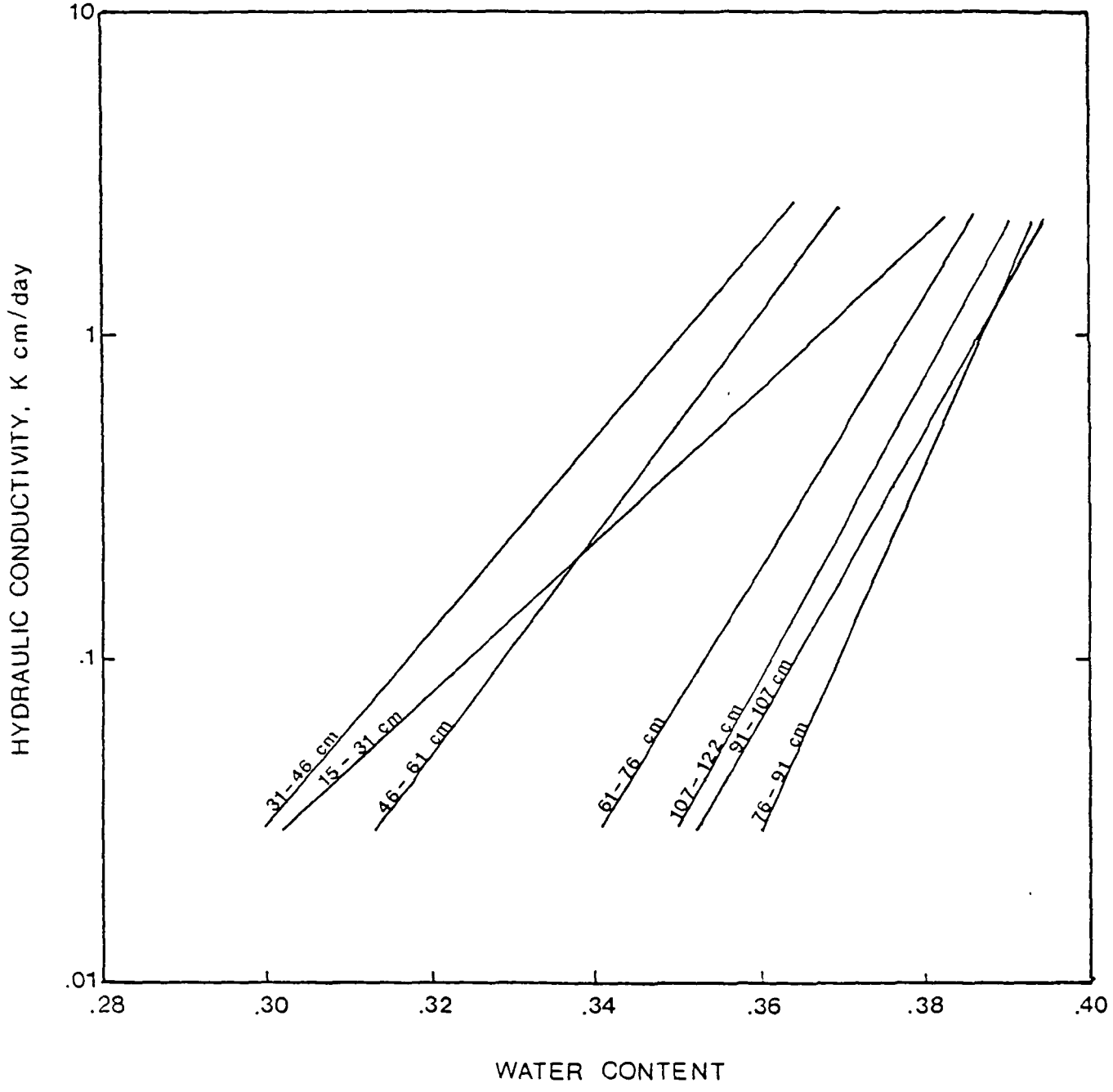

Figure 20. Hydraulic conductivity as a function of soil water content in 7 soil depth intervals.

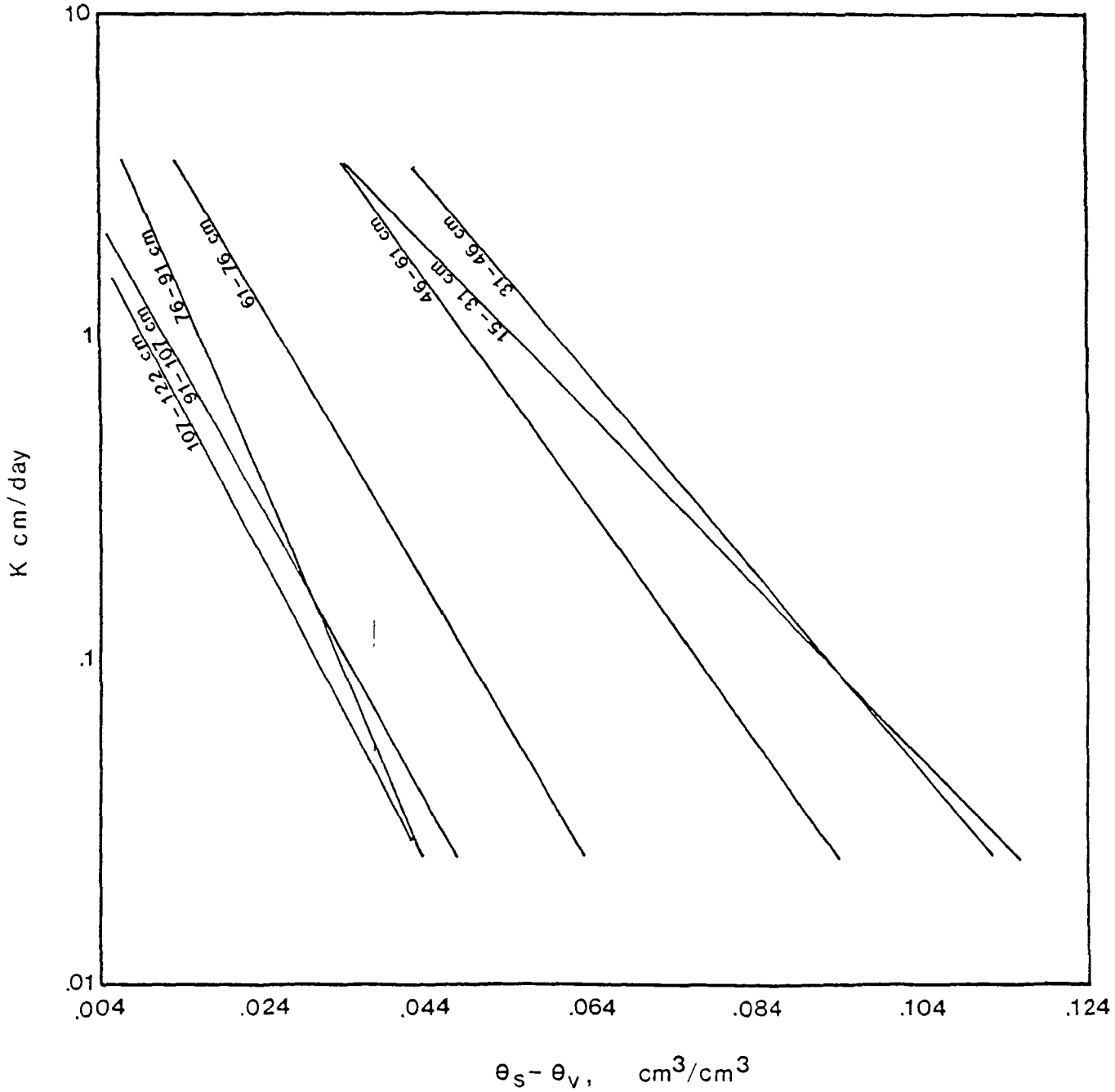

Figure 21. Hydraulic conductivity as a function of deficit volumetric water content from the saturation water content at various depth intervals.

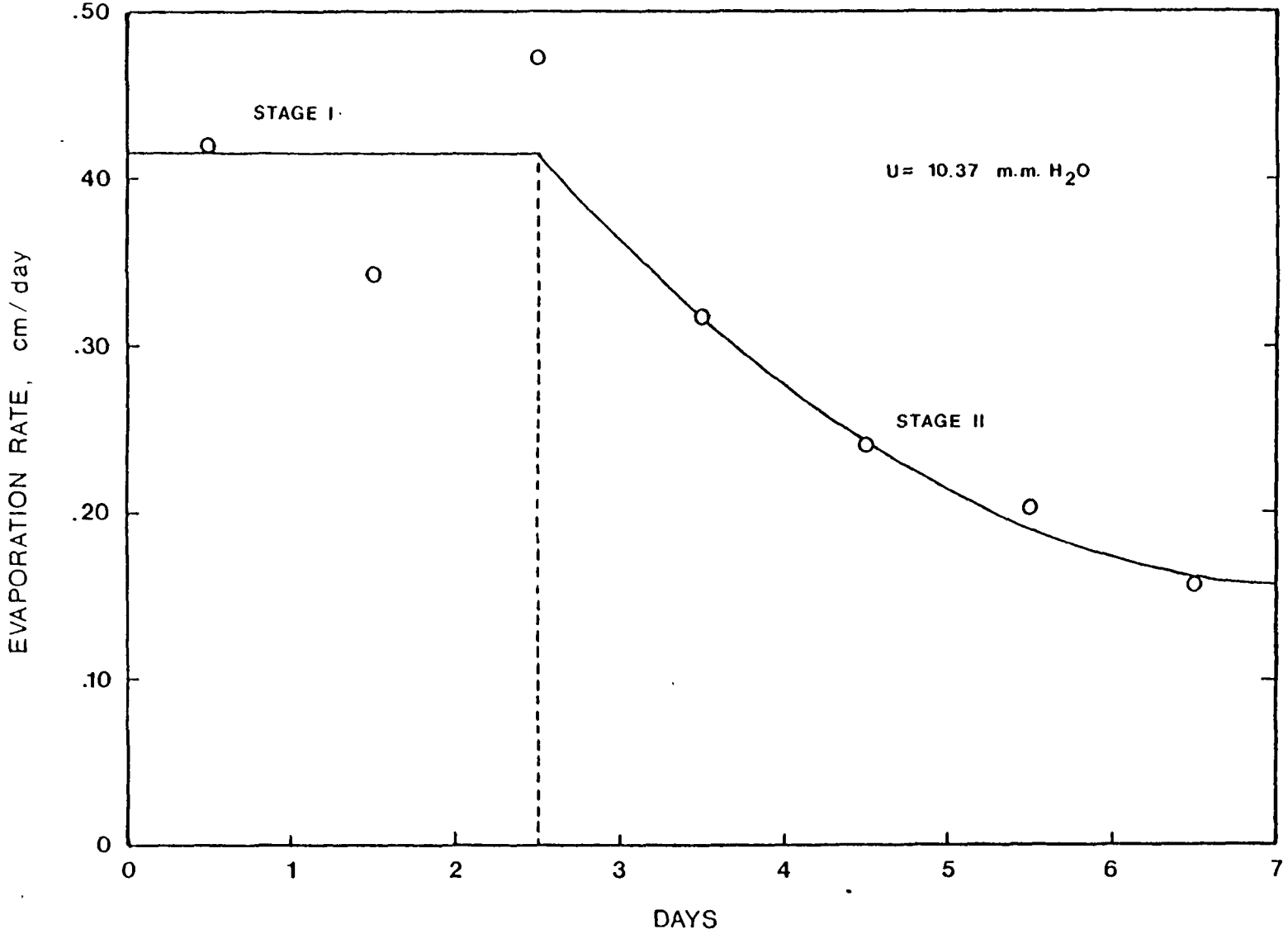

Figure 22. Evaporation rate, cm/day, as a function of time, during the drainage cycle.

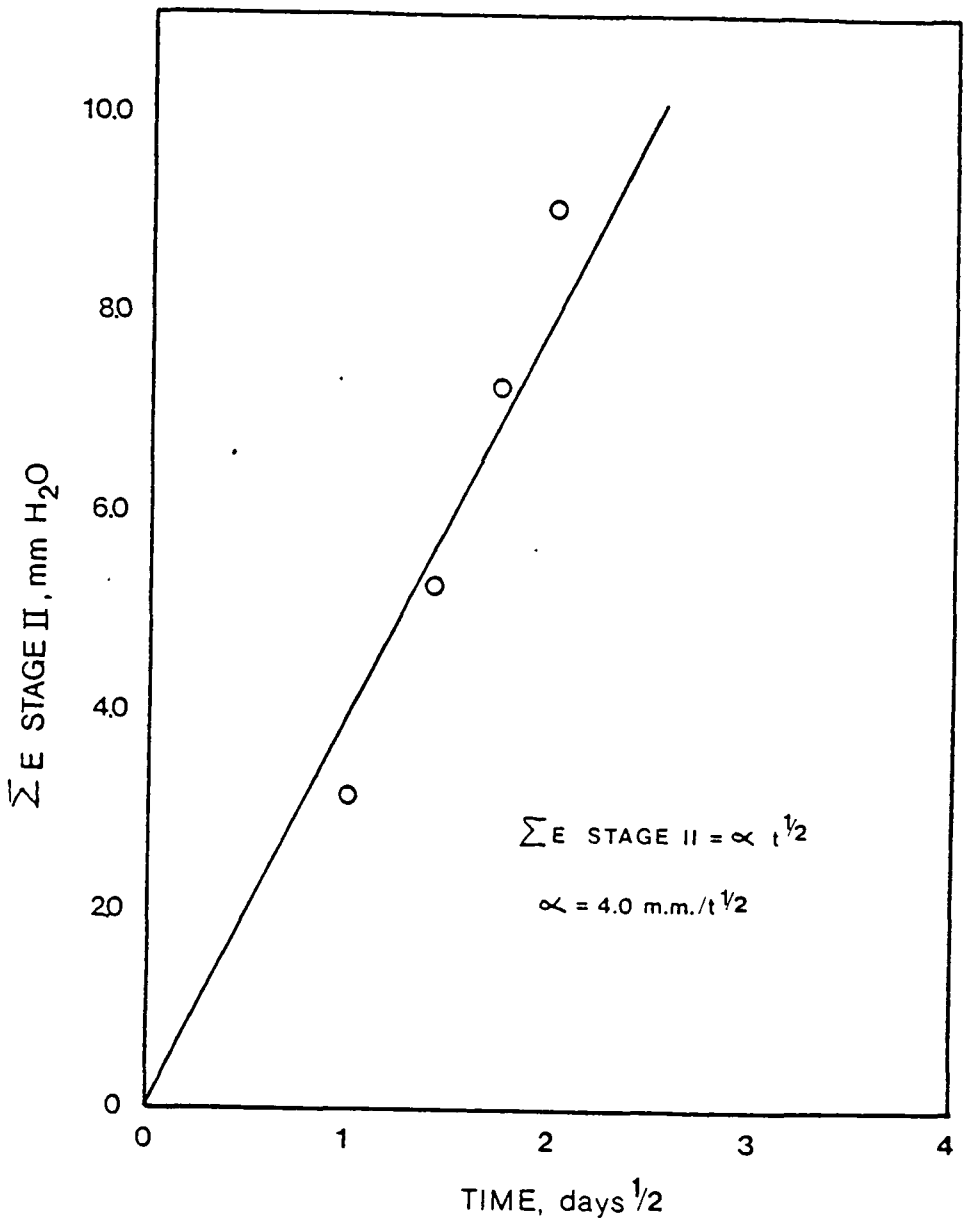

Figure 23. Cummulative evaporation rate for stage II as a function of (Time)½

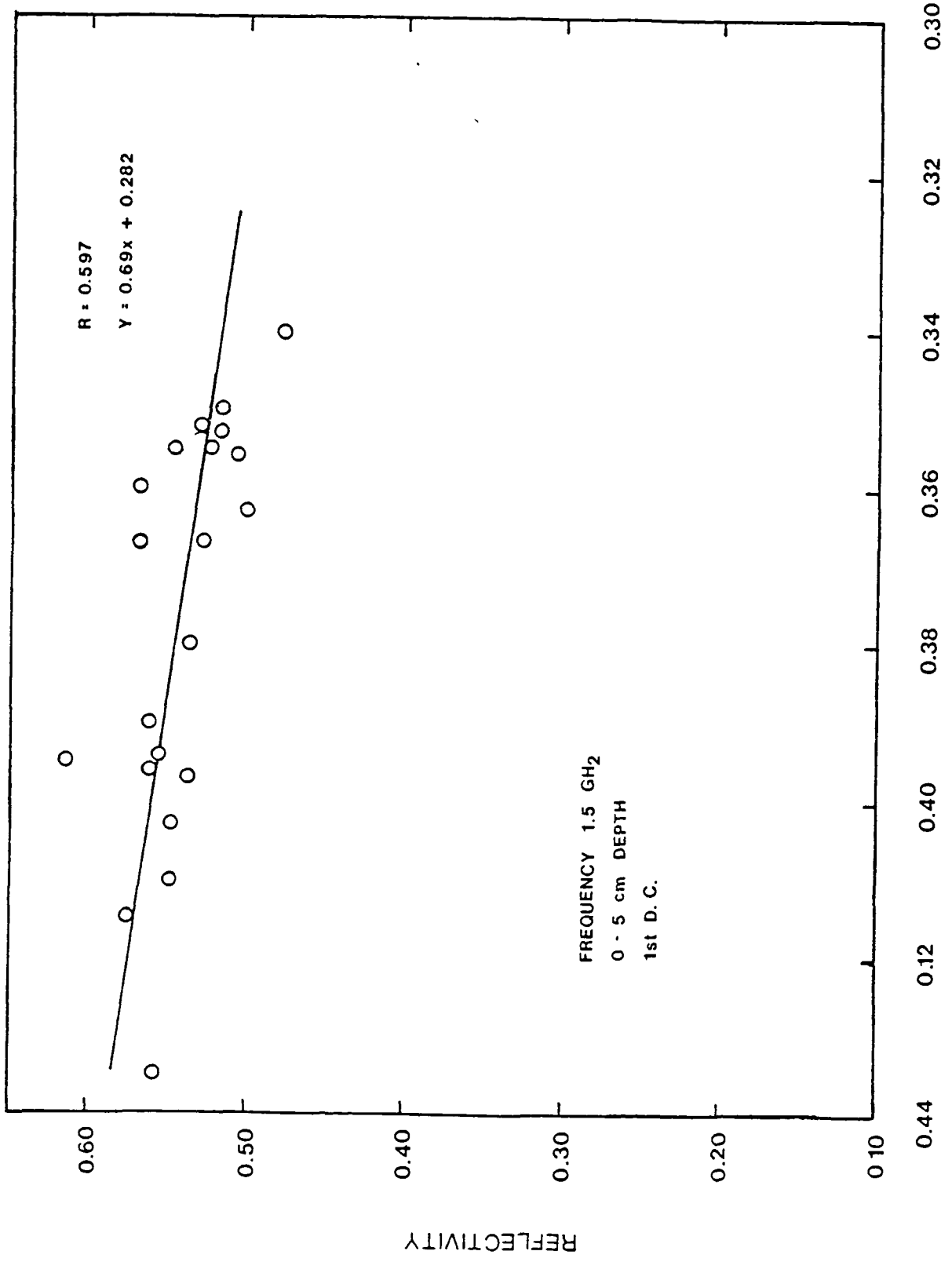

Figure 24. Relationships between reflectivity at frequency of 1.5 GH_2 and water content from moisture retention curve for 1st drainage cycle.

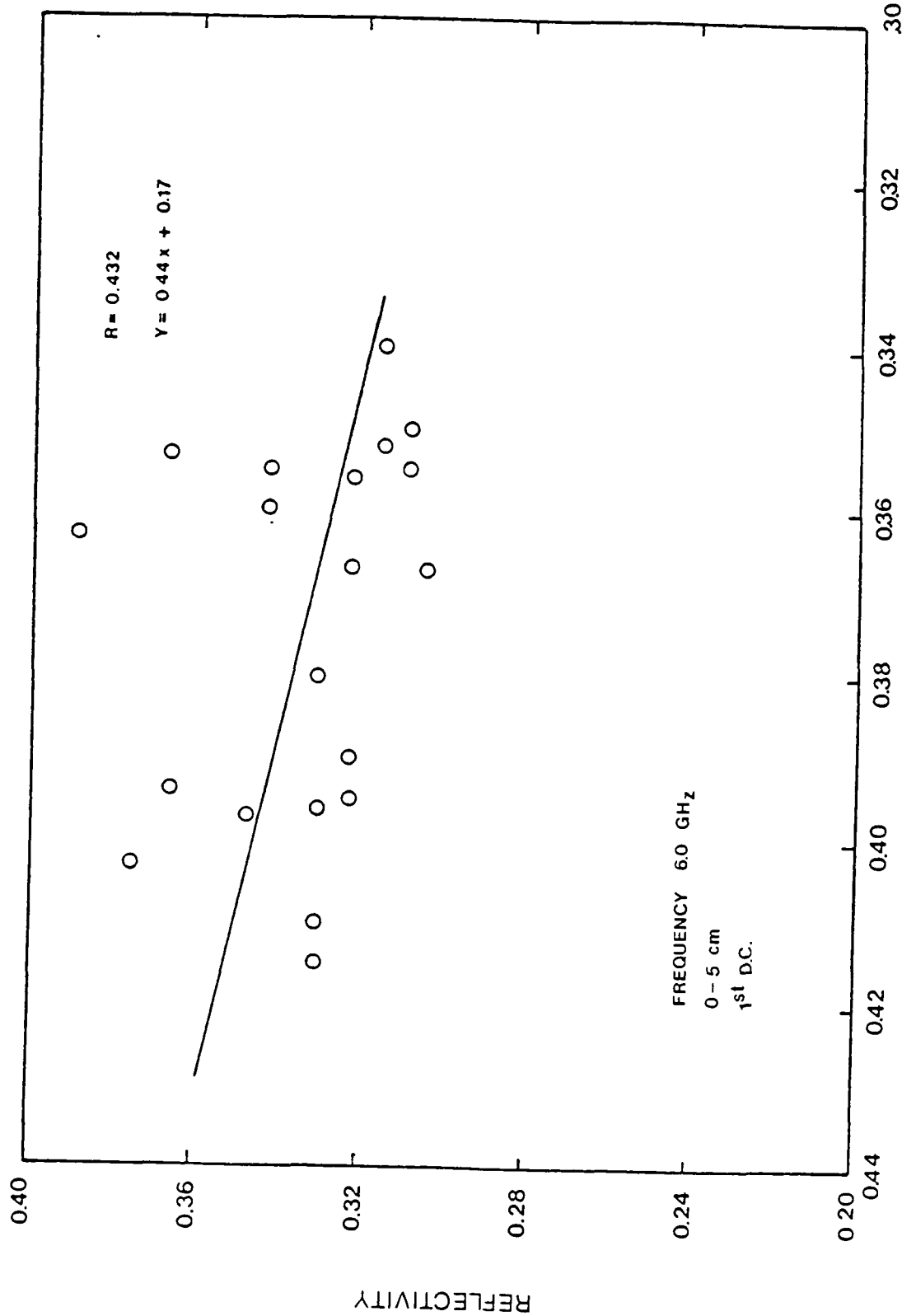

Figure 25. Relationships between reflectivity at frequency 6.0 GH_2 and water content for 1st drainage cycle.

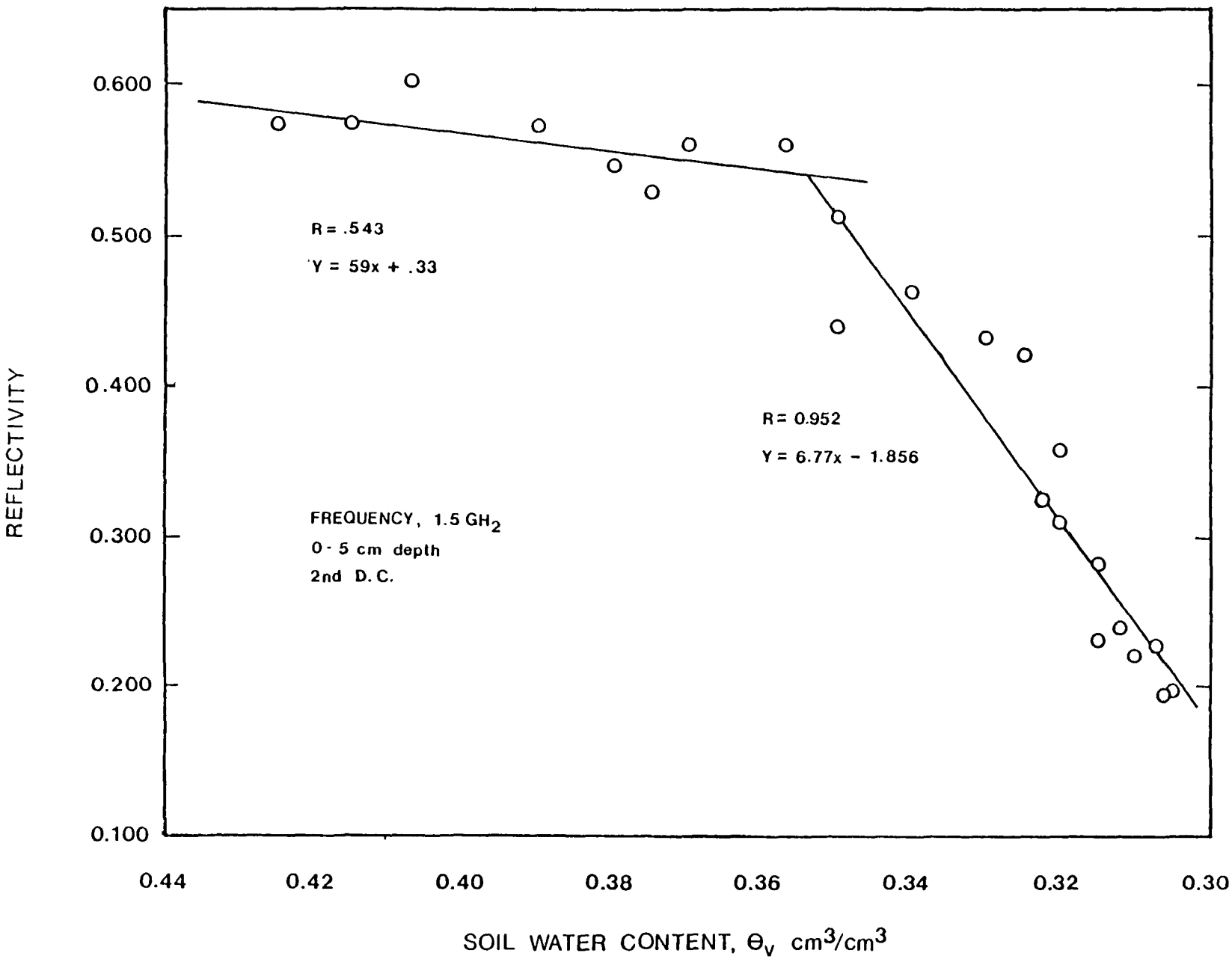

Figure 26. Relationships between reflectivity at 1.5 GH_2 frequency and water content for 2nd drainage cycle.

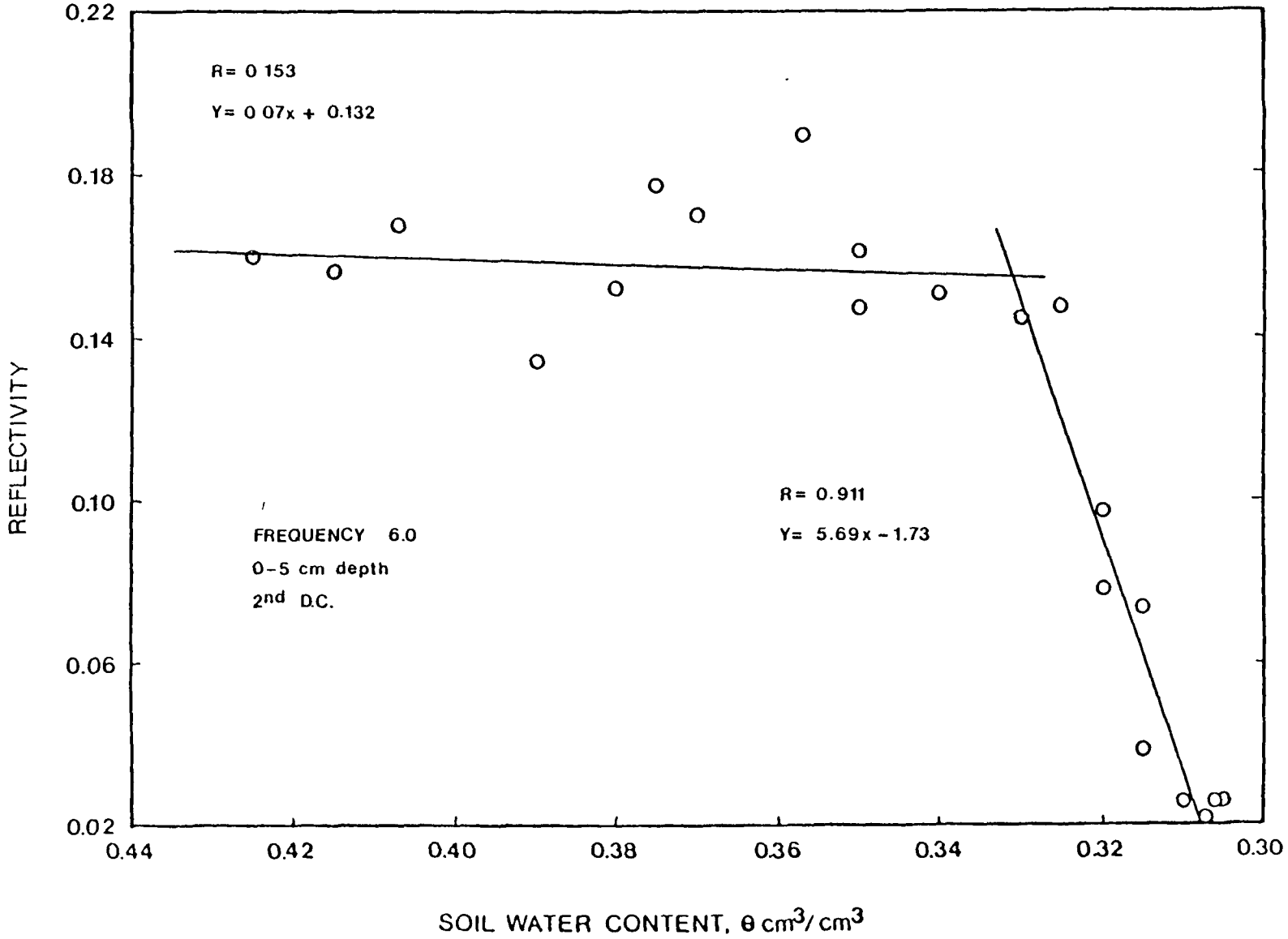

Figure 27. Relationships between reflectivity at 6.0 GH_2 and water content for 2nd drainage cycle.

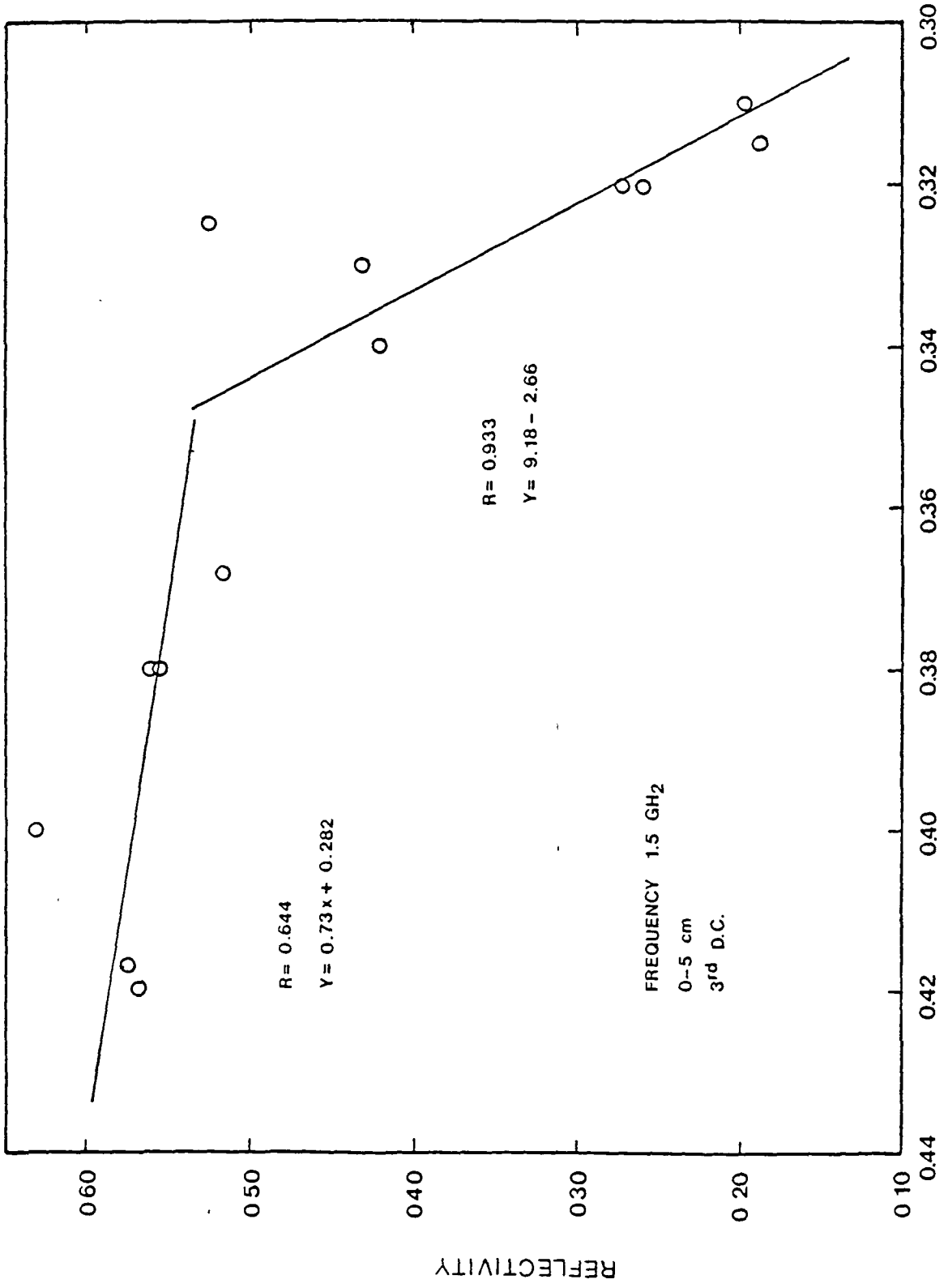

Figure 28. Relationships between reflectivity at 1.5 GH_2 and water content for 3rd drainage cycle.

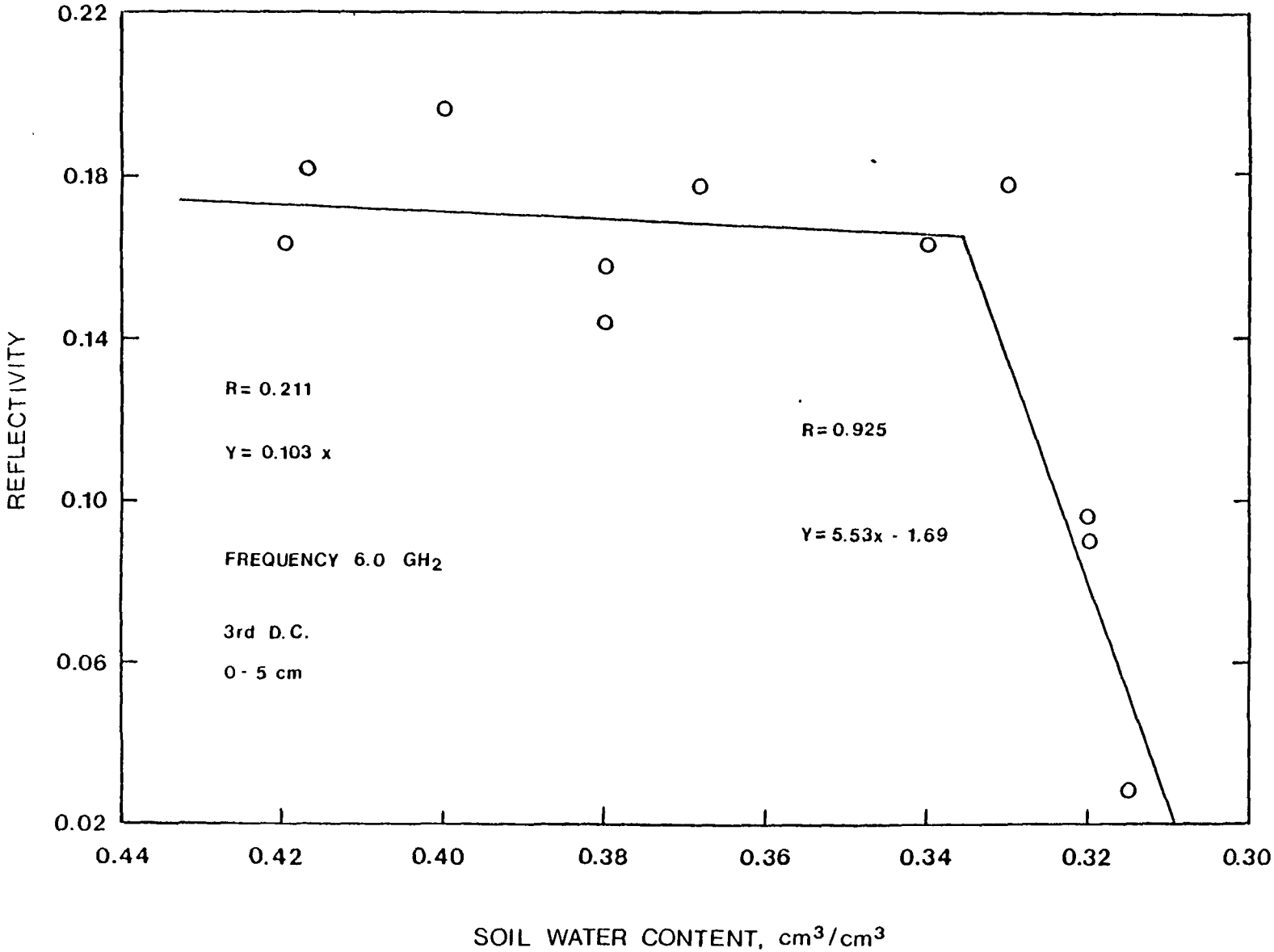

Figure 29. Relationships between reflectivity at 6.0 GH_2 and water content for 3rd drainage cycle.

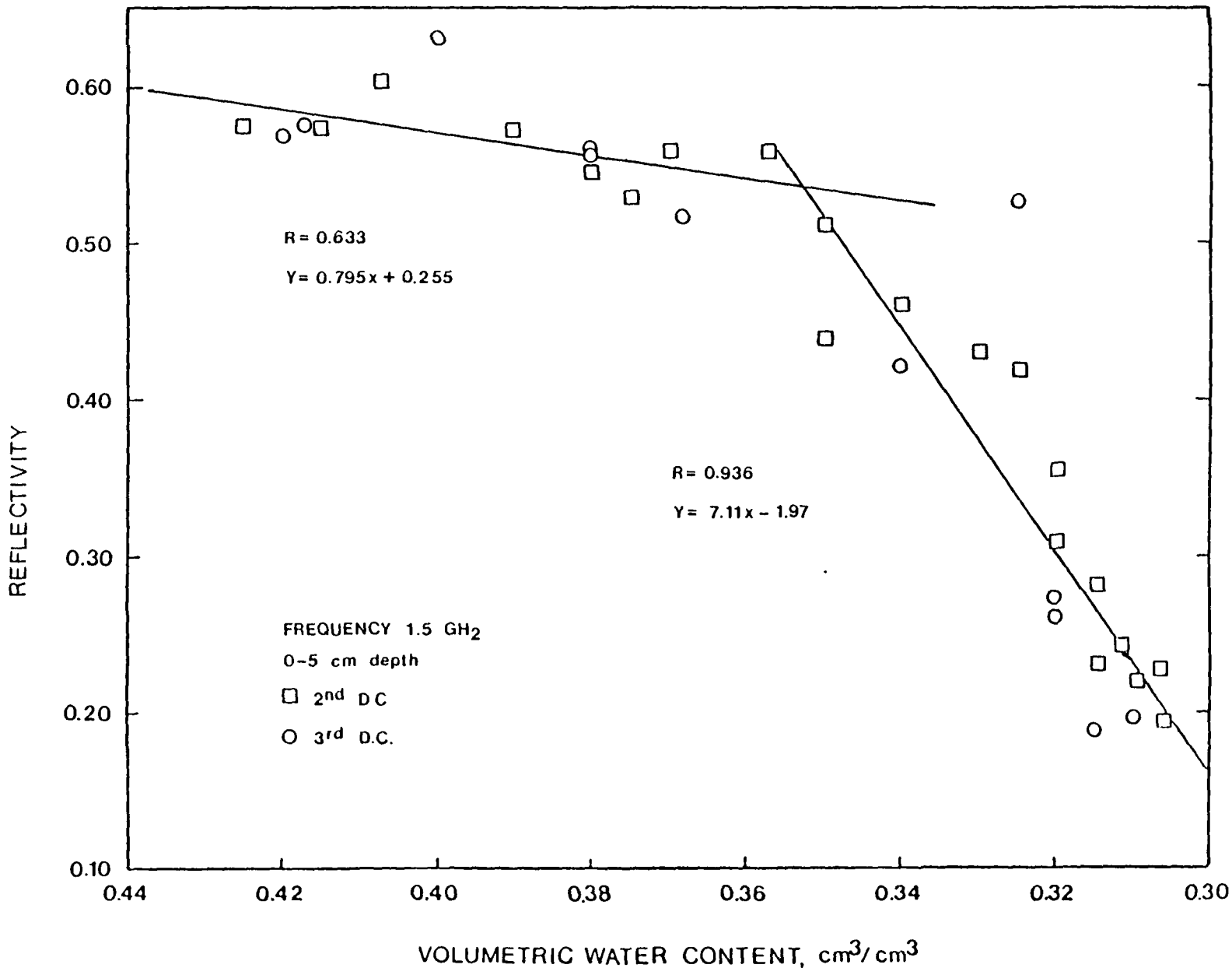

Figure 30. Relationships between reflectivity at 1.5 GH_2 and water content combining 2nd and 3rd drainage cycle.

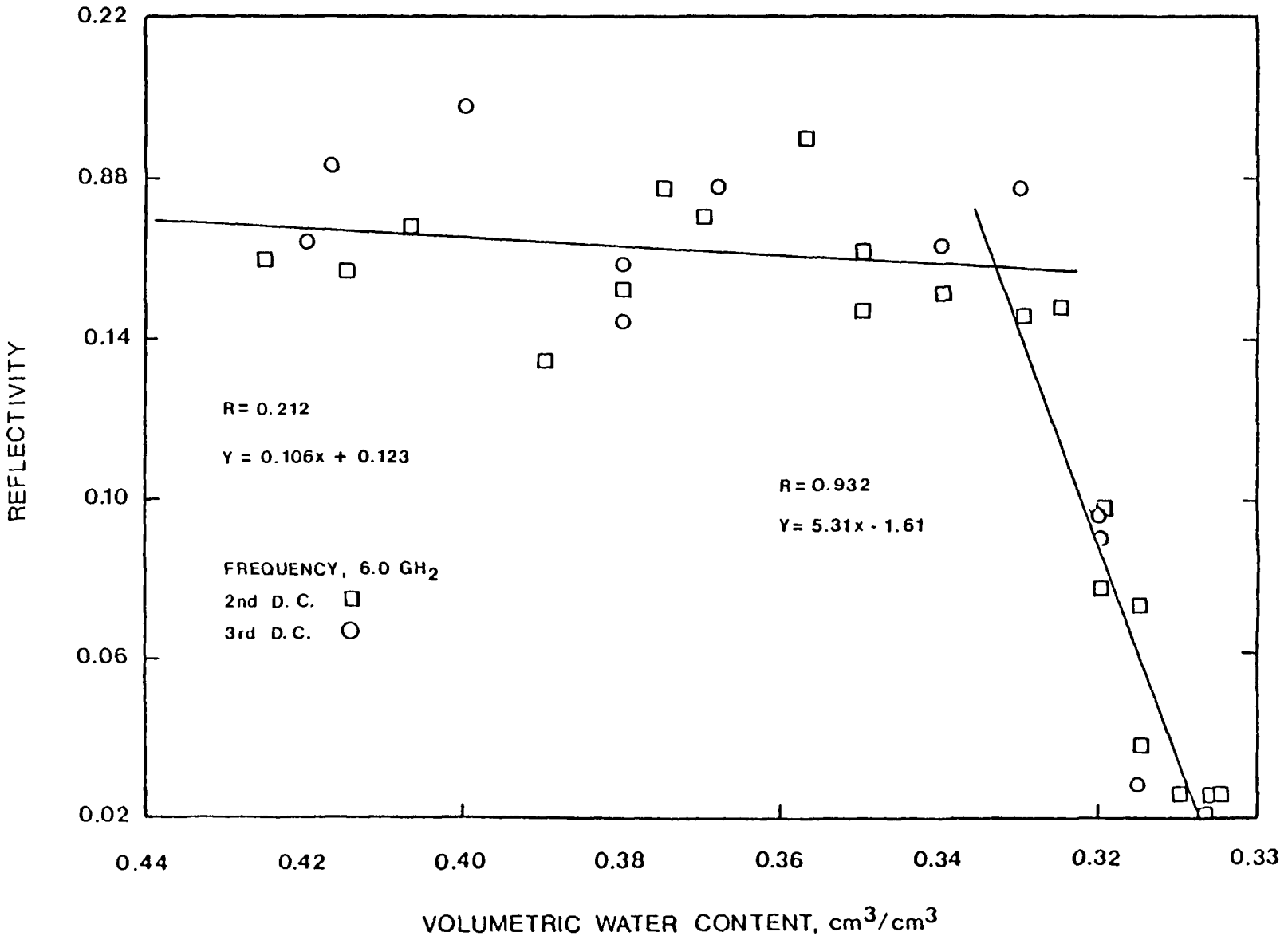

Figure 31. Relationships between reflectivity at 6.0 GH_2 and water content combining 2nd and 3rd drainage cycles.

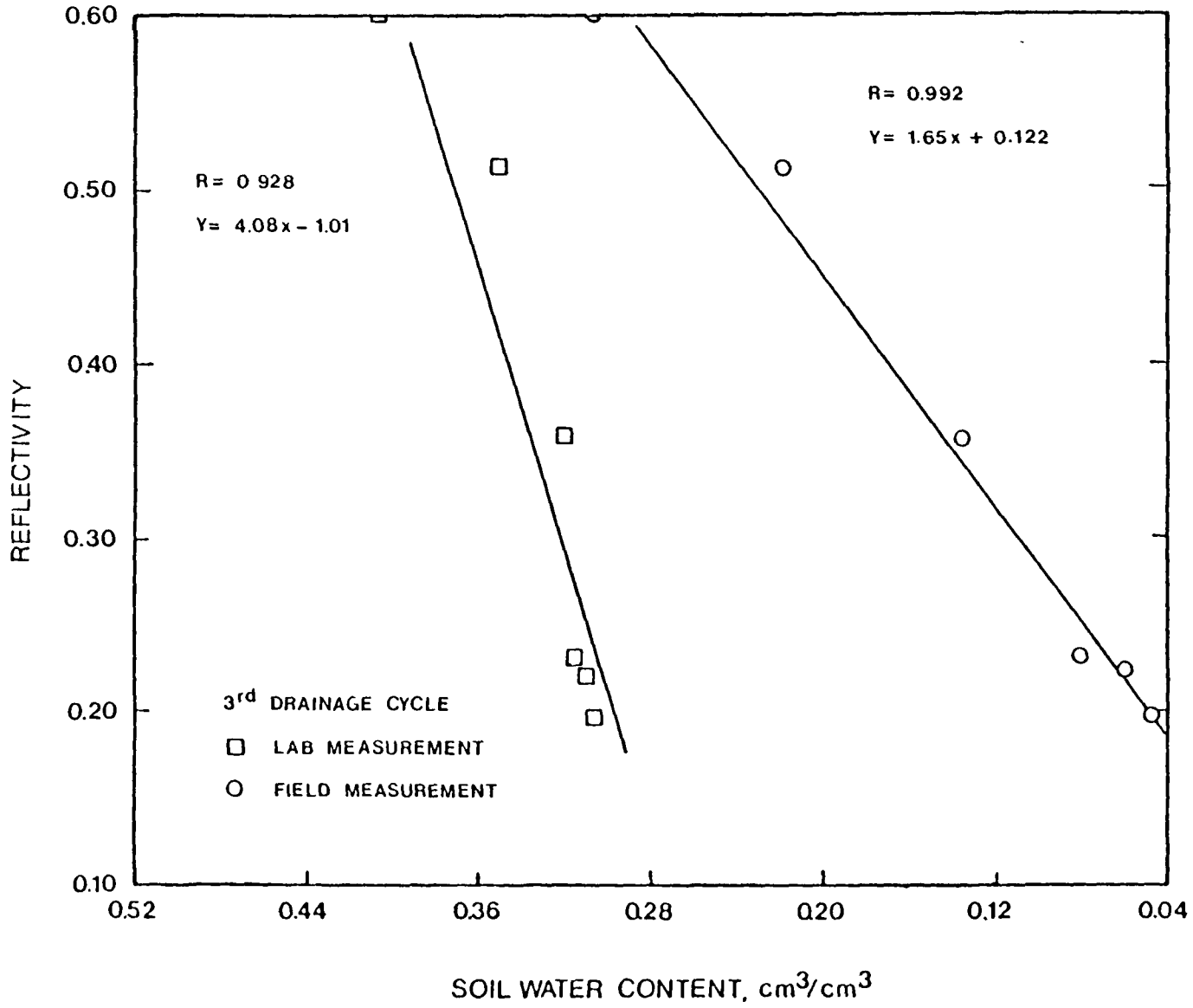

Figure 32. Change in reflectivity versus two different water content values.